The Gamma Ray Detection Capabilities of the Alpha Magnetic Spectrometer

R. Battiston[1], M. Biasini[1], E. Fiandrini[1],

J. Petrakis[2], and M.H. Salamon[2]

[1]Sezione INFN and Dipartimento di Fisica, Università di Perugia

[2]Department of Physics, University of Utah

Abstract

The modeled performance of the Alpha Magnetic Spectrometer (AMS) as a high-energy (0.3 to 100 GeV) gamma-ray detector is described, and its gamma-ray astrophysics objectives are discussed.

PACS, Keywords: 95.55.K, 98.54.C, 95.35.+d, 98.35.G; high-energy gamma rays, blazars, neutralinos, gamma-ray background

1 Introduction

Our knowledge of the γ-ray sky has increased dramatically during this last decade, due principally to the γ-ray instruments on board the Compton Gamma Ray Observatory (CGRO)[1]: EGRET, a spark chamber plus calorimeter instrument with γ-ray sensitivity in the energy interval 30 MeV to 30 GeV; COMPTEL, a Compton telescope in the interval 0.1 to 30 MeV; BATSE, an omnidirectional x-ray and soft γ-ray "burst" detector consisting of large NaI scintillators sensitive to 30 keV to 2 MeV photons (with smaller spectroscopic NaI crystals for measurements up to 110 MeV); and OSSE, consisting of Nai-CsI phoswiches detecting photons of 0.1 to 10 MeV. Their observations have revolutionized our understanding of such extragalactic phenomena as blazars and gamma ray bursts (GRBs), as well those within our own Galaxy, such as pulsars.

A salient characteristic of these extragalactic sources is their extreme time variability. In the case of blazars, flare states are observed to occur in which the luminosities vary by over an order of magnitude within time-scales as small as hours. GRBs are singular, extragalactic events due either to the the coalescence of massive compact objects or to the hypernovae of massive early stars, whose luminosities decay over periods of seconds to days depending upon the wavelength observed. For such objects, the importance of correlated, *multiwavelength* observations is paramount. By monitoring the relative time lags of blazar flare peaks at radio, optical, x-ray, and γ-ray wavelengths, for example, the properties of the source regions at the bases of AGN (active galactic nucleus) jets are constrained. Gamma ray observations of blazars by EGRET have been particularly crucial, as the luminosity of these objects peaks in the GeV-to-TeV part of the electromagnetic spectrum. The transient nature of these sources therefore argues for *continuous* coverage of the γ-ray sky.

Until recently, observations with CGRO and other space-based and ground-based telescopes have provided coverage of these and other sources up to the limiting sensitive energy of EGRET, approximately 30 GeV. From there, a gap in our knowledge of the γ-ray sky spectrum has existed up to 200-300 GeV, where ground-based γ-ray shower detectors presently have their energy thresholds. It is possible that within this gap there are novel features in the γ-ray sky, such as a gamma-ray line or continuum emission from postulated neutralino annihilation at the center of the Galaxy. Future instruments with sensivity in this unexplored region, such as AGILE [3],

recently approved by the Italian Space Agency (ASI), or the proposed GLAST [2] payload, may uncover exciting new phenomena.

At the present time, however, our view of the γ-ray sky has diminished. With the effective turnoff of the EGRET γ-ray instrument on the CGRO due to the nearly complete consumption of its spark chamber gas, there will soon be no operating instrument capable of observing the γ-ray sky in the energy interval $\sim 10^{-1}$ to $\sim 10^{2}$ GeV. Ground-based γ-ray detectors, based on the atmospheric Cerenkov technique (ACT)[4], turn on at current energy thresholds of $\sim$200-500 GeV. Within the next several years energy thresholds for some ACT observatories are expected to go to as low as 20 to 50 GeV, but lower thresholds than these are unlikely to be achieved due to the sizable effect of Earth's magnetic field on the γ-ray-induced air showers, and the lower Cerenkov photon yield which must be detected against the night sky background. For γ-ray energies much lower than 10^{2} GeV, then, spaced-based detectors are required. This observational gap for the energy window $\sim 10^{-1}$ to 10^{2} GeV will continue to exist for the next several years. Eventually, this gap will be eliminated with the launch of a next-generation γ-ray satellite, such as GLAST [2], but such a mission is unlikely to occur before the year 2005. Also the AGILE satellite [3], to be launched in 2002, will have a limited sensitivity above 50 GeV.

In this paper we describe how the Alpha Magnetic Spectrometer (AMS) can largely fill this gap by acting as a γ-ray detector with sensitivity in the energy interval of 0.3 to 100 GeV during its three-year mission on board the International Space Station Alpha (ISSA) from 2003 to 2006. AMS, described in detail elsewhere, has as its primary mission the search for cosmic ray antinuclei, which are detected via the negative curvature of their trajectories through a magnetic spectrometer (see Sect. 2).

It is of interest, however, to analyze if a large particle detector like AMS, operated on the Space Station for three years starting in 2003, could be used to detect high energy γ-rays . There are at least two ways this could be done without significantly affecting the experiment sensitivity to antimatter: a) adding a light (e.g. $0.3X_0$) converter at the entrance of the magnetic spectrometer, either passive (e.g., a high-Z thin plate) or active (e.g. a multilayer tracking detector), or b) implementing an high granularity imaging shower detector at the bottom of the experiment. Option (a) consists in a minor modification to the baseline instrument, while option (b), although

would give a much higher γ-ray detection capabilities, requires the addition of a new detector. In this paper we present a study which has been perfomed on option (a). We will show that in this option, AMS can also detect γ-rays with performance characteristics similar to EGRET in the energy region of 0.3 to 20 GeV, and with significantly enhanced capabilities between 20 and $\sim$ 100 GeV, a region which is not well unexplored. We refer to this modified instrument as "AMS/γ". We show that AMS/γ can continue the valuable work of EGRET by providing continued monitoring of extragalactic and galactic γ-ray sources and by participating in multiwavelength observational campaigns. In addition, AMS/γ will have unprecedented sensitivity to the γ-ray sky between the energies of 20 to $\sim$ 100 GeV (albeit at a level somewhat lower than required for detection of known sources with power law spectra), so that AMS/γ might provide us with unexpected discoveries in this region.

The next section gives a brief description of the baseline AMS instrument, and the modifications required for adding γ-ray detection capability in option (a). Section 3 describes the performance characteristics of AMS/γ determined from Monte Carlo analyses, and Section 4 uses these results to address the question of what γ-ray astrophysics can be done with AMS. The results obtained analyzing option (a) give a hint of the physics potential which could be reached implementing option (b) for the flight of AMS on the Space Station; option (b) would gain a factor of about 5 in γ-rays statistics over option (a). Detailed analysis of option (b), however, wil be the subject of future work.

2 The Alpha Magnetic Spectrometer

2.1 The Baseline Instrument

The Alpha Magnetic Spectrometer has been built by a large international collaboration of high energy physics institutions from the U.S., Italy, China, Finland, France, Germany, Taiwan, Russia, and Switzerland. It recently had a successful test flight on the Space Shuttle mission STS-91 in June, 1998 [79], where it was carried in the cargo bay and observed for several days in both the zenith and nadir directions, the latter for measurement of albedo cosmic ray backgrounds. It is scheduled to be secured to an external payload attachment point on the International Space

Table 1: AMS silicon tracker parameters (in parenthesis the values used on the precursor flight).

Number of planes	6
Accuracy (bending plane)	10 μm
Accuracy (non bending plane)	30 μm
Number of channels	163936
	(58368)
Power consumption	400 W
	(180 W)
Weight	130 kg
Silicon Area (double sided)	5.4 m^2
	(2.4 m^2)

Station Alpha in 2003, where it will remain as a zenith-pointing instrument for a minimum of 3 years.

The basic design of AMS is shown in Figure 1. The magnet spectrometer consists of a permanent ring dipole magnet made of very high grade Nd-B-Fe rare earth material whose magnetic energy product and residual induction are respectively $(BH)_{\max} > 50 \times 10^6$ G-Oe and 14,500 G, yielding an analyzing power of $\langle BL^2 \rangle = 0.14$ T-m^2 with less than 2 tonnes of magnet mass.

Four silicon strip detector tracking planes are located within the magnetic volume, with a fifth and sixth plane located just above and below the magnet. These are based on technology developed for the Aleph and L3 vertex detectors at LEP [5], and consist of 300μm thick, double-sided, high purity silicon wafers. The total area of this tracker is about an order of magnitude larger than the size of previous microstrip silicon detectors. The momentum resolution of the silicon spectrometer is given in Figure 2 at low rigidities (below 8 GV) the resolution is dominated by multiple scattering ($\Delta p/p \sim 7\%$), while the maximum detectable rigidity ($\Delta p/p \sim 100\%$) is about 500 GV. The parameters of the silicon spectrometer are given in Table 1. In addition to measuring particle rigidity, the silicon planes will provide six independent measurements of dE/dx for charge determination.

Four time-of-flight (ToF) scintillator planes (two above and two below the magnet volume) measure the particle velocity with a resolution of 120 ps over a distance of 1.4 m. The ToF scintillators also measure dE/dx, allowing a multiple determination of the absolute value of the particle charge.

A solid state Cerenkov detector below the magnet provides an independent velocity measurement. In addition, a scintillator anticounter system is located within the inner magnet wall, extending to the ToF scintillators.

The performance of this instrument as a nuclear cosmic ray detector, and its sensitivity to an antinucleus cosmic ray component, is discussed elsewhere[6].

We should also note that by the time AMS is attached to the International Space Station it may have undergone significant changes from the baseline design considered here. In particular, the permanent magnet may be replaced by a superconducting magnet, which would considerably improve AMS's γ-ray detection performance (although it would increase the γ-ray energy threshold as well; see 3.3). Since the detector is still undergoing significant design changes from the baseline instrument flown on the Space Shuttle, we have chosen to fix on that design which currently exists as integrated hardware. The addition of other components, such as a transition radiation detector, a segmented calorimeter, a solid Čerenkov radiator, and/or a superconducting magnet will only improve the performance of AMS/γ described in this paper.

2.2 Modifications of AMS for γ-ray Detection

In option (a), the conversion of AMS to AMS/γ requires the addition of two hardware components: (1) A high-Z converter plate (*e.g.* tungsten) of 0.3 radiation lengths ($x = 0.3X_0$), which converts γ-rays into electron-positron pairs. The momenta of each electron and positron are measured in the spectrometer, and their weighted sums give the primary photon's energy and incidence direction. (2) A stellar attitude sensor gives the angular orientation of AMS with respect to the celestial sphere to an accuracy of better than 1.5×10^{-4} radians. The stellar attitude sensor is required because the Space Station cannot provide attitude information to better than $\sim 2^\circ$, while the AMS/γ angular resolution approaches $1'$ for $E\gamma > 100$ GeV. Commercial units, such as Ball Aerospace Systems Division's CT-633 Stellar Attitude Sensor, provide angular resolutions to $0.5'$

with very modest weight and power consumption (2.5 kg and < 10 W).

Determination of the converter thickness and position is based on the following considerations:
(1) The γ-ray converter must not degrade the sensitivity of AMS for antimatter detection. Therefore the converter mass cannot be distributed uniformly throughout the tracking volume, which would otherwise provide optimal angular and energy resolution. Instead, the converter must lie as a single plate just above the second TOF scintillator, S2.
(2) The loss of nuclear antimatter candidates to nuclear interactions in the converter plate must be insignificant: At $x = 0.3X_0$, this amounts to only $\sim 2\%$ of cosmic-ray ^{4}He being lost.
(3) The sensitivity for detection of astrophysical point sources of gamma rays is nearly independent of x for $x \ll X_0$ for background-limited (as opposed to statistics-limited) detection. This sensitivity degrades as $x/X_0 \to 1$.
(4) The aperture for rare events and for measurement of the diffuse gamma ray background increases with x.
(5) The fractional energy loss of the electron pair due to bremsstrahlung within the converter is $\propto x/X_0$, degrading energy resolution as x increases.
(6) Can the presence of the converter plate create background that will degrade the cosmic ray $\overline{\text{He}}$/He target sensitivity of 10^{-9}? By requiring clean tracks in the spectrometer volume we do not expect converter-generated contamination, as the converter lies above the magnet volume. This is corroborated both by the SHuttle flight data (where an $\overline{\text{He}}$/He of $\sim 10^{-6}$ was obtained [79]) and by Monte Carlo analyses. This question is also being examined using helium and carbon data from GSI at Darmstadt.

For this anaysis we choose the value $x = 0.3X_0$, for which point source sensitivity is still optimal, the energy resolution is acceptable, and nuclear interaction losses are negligible.

3 The Performance of AMS/γ

3.1 Monte Carlo Calculations

A full-instrument GEANT Monte Carlo code was run to determine the performance of AMS/γ. Gamma rays with fixed energies, ranging from 0.3 to 100 GeV, were thrown isotropically at the detector over an opening angle of 50°.

For those γ-rays which converted in the detector (most within the converter plate) the charged particles were tracked through the inhomogeneous field of the ring dipole permanent magnet. The inhomogeneous field used was that measured for the AMS magnet that was recently flown on the Space Shuttle (flight STS-91), with a field strength increased by 7% to match the expected field strength of a second magnet which might be constructed for the Space Station mission.

All the physical processes for electrons and γ-rays were "on" in the GEANT code. Bremsstrahlung photons of energies < 20 MeV were not followed, although all bremsstrahlung energy losses were included. The hit positions in the silicon tracker planes were assigned gaussian errors with $\sigma = 15\mu$m and 30μm for the bending and nonbending planes, respectively. (Test beam measurements give a bending plane Si tracker resolution below 10 μm [7].) Reconstruction of the particle trajectories were performed with a quintic spline fit routine [8] to determine their momenta and charge sign. Assignment of a hit position within the 6-plane Si tracker to either the converted electron or positron was done for all possible combinations (64 in all) of assignments; that combination whose trajectory reconstruction χ^2 was minimum was selected as the event. All secondary charged particles were tracked in the detector volume until they stopped or exited from the detector mother volume.

The γ-ray candidate events were those that passed the hardware trigger of $\overline{S1}\cdot S2\cdot S3\cdot S4$, where $S1$ to $S4$ are the ToF counters (the converter plate lies between $S1$ and $S2$). If reconstruction of particle trajectories occurred successfully, further cuts were placed on these candidate events before acceptance as a γ-ray event:

1) the reconstructed γ-ray zenith angle θ_γ must be $\leq 50°$;

2) the reconstructed γ-ray energy E_γ must be ≥ 0.15 GeV;

3) there are at least two reconstructed tracks;

4) the reconstructed energy of the most energetic particle be ≥ 0.15 GeV;

5) the number of anticoincidence panels hit (there are 16 such panels along the interior wall of

the magnet) be < 4.

Primary γ-ray energy and incidence direction were determined by adding the fitted momenta vectors of all secondaries evaluated at the converter plate to obtain the primary momentum vector. (More sophisticated weighting methods were found to have negligible effect on γ-ray angular resolution.) The results of the Monte Carlo runs are discussed in the subsections below.

3.2 Point Source Sensitivity

Astrophysical sources of γ-rays fall into two categories: point sources, such as blazars and GRBs, and diffuse sources, such as the cosmic isotropic γ-ray background and possibly γ-ray emission from neutralino annihilation near the center of our Galaxy. Some galactic sources fall into an intermediate category of "extended" sources, such as pulsar nebula and supernova remnants, where the source angular size may be larger than the point spread function of the γ-ray detector.

For point sources, a detector's key figure of merit is its *point source sensitivity*, defined as the minimum source flux required to achieve a specified level of detection significance. The significance S of a detection is given schematically by

$$S(> E_{\rm t}) \sim \frac{N(> E_{\rm t})}{B(> E_{\rm t})^{1/2}}, \tag{1}$$

where $N(> E_{\rm t})$ and $B(> E_{\rm t})$ are respectively the total number of detected photons from the source and the number of background photons falling within the source area above an energy $E_{\rm t}$. $E_{\rm t}$ is usually, but not always, the instrument's threshold energy. N and B are a function of the effective detection area $A(E)$ of the instrument, its angular resolution expressed as a solid angle $\Omega(E)$, the viewing time t, and the differential source and background spectra dN/dE and dB/dE:

$$N(> E_{\rm t}) = \int_{E_{\rm t}}^{\infty} \frac{dN}{dE} A(E) t \, dE, \tag{2}$$

and

$$B(> E_{\rm t}) = \int_{E_{\rm t}}^{\infty} \frac{dB}{dE} A(E) \Omega(E) t \, dE. \tag{3}$$

All extragalactic objects (blazars) seen by EGRET are well-represented by power law spectra

$$\frac{dN}{dE} = n_0 \left(\frac{E}{1{\rm GeV}} \right)^{-\gamma} ({\rm cm}^2 \cdot {\rm s} \cdot {\rm GeV})^{-1}, \tag{4}$$

where γ is the differential spectral index of the source, and n_0 is the differential flux at 1 GeV. We define our point source sensitivity as that value of n_0 which gives a 5σ signal integrated over the period of one year of operation of AMS. It is evident that the point source sensitivity is a function of the source's spectral index; for these calculations we have assumed a source differential spectral index of $\gamma = 2$, which is close to the mean of the source spectral indices of blazars observed by EGRET [9].

The background flux dB/dE contains components from the isotropic extragalactic γ-ray background radiation and from the galactic diffuse radiation (the latter due to the decay of π^0s produced in collisions of cosmic rays with the interstellar medium). The former has recently been determined by EGRET to be [10]

$$\frac{dB_{\rm extragal}}{dE} = (7.32 \pm 0.34) \times 10^{-6} \left(\frac{E}{0.451 \text{ GeV}}\right)^{2.10\pm0.03} (\text{cm}^2 \cdot \text{s} \cdot \text{sr} \cdot \text{GeV})^{-1}. \tag{5}$$

The galactic diffuse radiation is a strong function of position in the sky, and been measured and modelled by the EGRET group [11]. We have used here their data to generate background spectra $\frac{dB}{dE}(E, \delta, \alpha)$ over 3° bins in declination δ and right ascension α.

The solid angle $\Omega(E)$ over which the background must be integrated when viewing a source is given by $\Omega(E) = \pi\sigma_{68}^2(E)$, where σ_{68}, following EGRET's usage, is defined as the angular radius within which 68% of the source photons fall. The converter thickness of 0.3 X_0 largely dominates all multiple scattering effects, so that the angular and energy resolution of reconstructed primary photons will be completely dominated by multiple Coulomb scattering (MCS) and bremsstrahlung energy losses of the electrons within the converter plate. Figure 3 confirms that the Monte Carlo result for AMS/γ's angular resolution is very close to that estimated from MCS within the converter plate:

$$\sigma_{68}^{\rm AMS}(E) = 0.88^\circ \left(\frac{E}{1 \text{ GeV}}\right)^{-0.956}, \tag{6}$$

which is to be compared to EGRET's angular resolution [12] of

$$\sigma_{68}^{\rm EGRET}(E) = 1.71^\circ \left(\frac{E}{1 \text{ GeV}}\right)^{-0.534}. \tag{7}$$

The effective area $A(E)$ of the instrument is also a function of the zenith angle θ of the incident photon, as shown in Figure 4 for 3 GeV photons. Although the θ dependence of the conversion

probability cancels that of the projected area, the requirement that $S3$ and $S4$ ToF scintillators be hit causes the effective area to drop to zero for $\theta > 50°$. An integration of effective area $A(E, \theta)$ over solid angle gives instrument aperture, shown in Figure 5. Below a γ-ray energy of 0.3 GeV, the converted electrons begin to have too small a radius of curvature to escape from the magnet volume, and detection efficiency plummets. Above 100 GeV the converted electron and positron often do not spatially diverge beyond the two-hit resolution distance of the silicon trackers, causing significant deterioration in γ-ray energy resolution. These then define the limits of the energy window for AMS/γ.

Because AMS will be rigidly attached to the ISSA which itself will be in 51.6° inclination orbit, AMS will not spend equal amounts of time viewing all directions in the celestial sphere. However, AMS/γ has finite detection area out to $\theta = 50°$, so that AMS/γ does view the entire sky. Full sky coverage is obtained roughly every three months due to the precession of the orbital plane of the Space Station about Earth's pole [13]. Because of this precession, the viewing area×time product over the sky is only a function of E and declination δ, and not of right ascension α. By following the orbit of AMS over one year, at each time element determining the $A\Delta t$ increment for each position in the sky viewable by AMS at that time, a total $At(E, \delta)$ area×time product is obtained, and is shown in Figure 6.

With the above results and Eqs. 2-6, AMS/γ's 5σ point source sensitivity can be obtained. The significance is calculated using the likelihood ratio of Li and Ma [14],

$$S = \sqrt{(2)} \left\{ N_{\rm on} \ln \left[\frac{1+\alpha}{\alpha} \left(\frac{N_{\rm on}}{N_{\rm on} + N_{\rm off}} \right) \right] + N_{\rm off} \ln \left[(1+\alpha) \left(\frac{N_{\rm off}}{N_{\rm on} + N_{\rm off}} \right) \right] \right\}^{1/2}, \qquad (8)$$

where $\alpha \equiv t_{\rm on}/t_{\rm off}$, $t_{\rm on}$ being the time spent viewing the source, and $t_{\rm off}$ being the time spent viewing off-source, and $N_{\rm on}$ and $N_{\rm off}$ are the total integrated on-source (signal plus background) and off-source (background) photon counts. Since at 1 GeV roughly 10^{-3} of the instrument's field-of-view (FOV) is contained in the σ_{68} error circle, we take $\alpha = 10^{-3}$. For any given position in the sky, that computed value of n_0 which gives $S = 5$ at 1 GeV is the point source sensitivity for that sky position. Figure 7 shows the one-year point source sensitivity for a lower cutoff energy $E_{\rm t}$ of 1 GeV.

One cannot directly compare the point source sensitivity of AMS/γ to that of EGRET, since AMS is not a pointable instrument. EGRET achieves a flux sensitivity of $I_{\rm min}(> 0.1 \text{ GeV}) \approx$

$10^{-7}\mathrm{cm}^{-2}\mathrm{s}^{-1}$ with a 2-week viewing period. Since it took EGRET one year to map the full sky, where each sky segment was viewed for roughly 2 weeks, we can compare EGRET's sensitivity with that achieved by AMS/γ after one year of operation. By assuming a source differential spectrum of E^{-2}, we can convert from EGRET's definition of sensitivity (in terms of integral flux above 0.1 GeV) to that of AMS/γ (a differential flux above 1 GeV). In our units the EGRET 5σ flux sensitivity is 1×10^{-8}. Over most of the sky, AMS/γ's mean sensitivity $\langle n_0 \rangle$ is estimated to be about a factor of 2 lower than that of EGRET.

3.3 Energy Resolution

The γ-ray energy resolution is dominated by bremsstrahlung losses in the converter plate, which have an average value of $\left\langle \frac{\Delta E}{E} \right\rangle \approx \frac{1}{2}\left(\frac{7\tau}{9X_0 \cos\theta}\right) \approx 0.16/\cos\theta$ for a converter thickness $\tau = 0.3X_0$. In the reconstructed γ-ray energy distributions for primary energies of 0.3, 3, 20, and 100 GeV, shown in Figure 8, one sees the effect of bremsstrahlung losses in the converter plate in the large low-energy tails of the distributions. The nearly identical appearances of these distributions is a consequence of the fact that the probability for the electron to radiate a fraction ν of its energy as a bremsstrahlung photon is solely a function of ν. There are two noticeable deviations from this universality in the figure: The cutoff of events below 0.1 GeV is due to the gyroradii of the electrons becoming smaller than the magnet field volume dimensions; the broadening of the distribution at 100 GeV is due to the fact that trajectory reconstruction errors are beginning to dominate bremsstrahlung losses in the energy determination. Figure 9 gives the mean fractional energy loss and the rms energy resolution as a function of primary γ-ray energy, and shows the deviations from constant values below 1 GeV and near 100 GeV.

That the reconstructed energy distributions have a nearly "universal" form has important consequences for the determination of blazar energy spectra. If a source energy spectrum follows a power-law energy distribution, $E^{-\gamma}$, and if the energy resolution function of the detector is of the form $f(E', E) = E^{-1}g(E'/E)$, where E is the true incident energy, E' is the reconstructed energy, and $g(x)$ is an arbitrary function of x, then the reconstructed source spectrum is also a power-law spectrum *with the same spectral index*. There will therefore be little bias in our reconstructed spectral indices. This is demonstrated in Section 4.1.2 (Figure 11) where the measured spectra of

several blazars, a convolution of the primary γ-ray energy spectrum $E^{-\gamma}$ and the energy resolution function $f(E', E)$, are seen to match the true spectra.

3.4 Comparison of AMS/γ with EGRET

The table below summarizes the performance characteristics of AMS as a γ-ray detector. In particular, by its comparison to EGRET, one sees that the two instruments perform similarly in many respects, one major difference being the energy windows: AMS's energy window is shifted up by roughly one order of magnitude from that of EGRET, thereby providing an improved view of the sky in the region $E_\gamma \sim 100$ GeV.

	AMS	EGRET
technique	magnetic spectrometer	spark chamber plus calorimeter
energy window (GeV)	0.3 to 100.	0.03 to 30.
peak effective area (cm^2)	1300	1500
angular resolution	$0.77°(E/1GeV)^{-0.96}$	$1.71°(E/1GeV)^{-0.534}$
half-area zenith angle	$\sim 30°$	$\sim 20°$
total viewing time (yr)	$\sim$3	$\sim$2
attitude capability	fixed	movable
flux sensitivity (ph/cm^2-s-GeV at 1 GeV)	$\sim 0.5 \times 10^{-8}$	$\sim 1.0 \times 10^{-8}$

A few of the table entries require some amplification: (1) The 30 GeV upper limit listed for EGRET is due in part to the effects of electromagnetic backsplash from their calorimeter into their hardwired anticoincidence scintillator shield that surrounds the instrument. Above $\sim$GeV energies this self-induced veto reduces EGRET's aperture roughly as $E^{-0.5}$. Although the EGRET collaboration quotes 30 GeV as their maximum energy, in fact they have small but finite aperture up to and beyond 100 GeV. (2) The total viewing time for EGRET is listed as 2 years. This takes into account the fact that, on average, during approximately one-third of the viewing time the pointing direction is occulted by Earth. (3) Unlike EGRET, AMS/γ is not a pointing instrument; its vertical axis is always aligned with the zenith. Therefore AMS/γ cannot point to targets of

opportunity.

Note that the point source sensitivity is nearly the same for both EGRET and AMS, with that of AMS being somewhat (factor $\sim$2) lower (given the caveat of Section 3.2). This is because EGRET and AMS have similar effective detection areas and angular resolutions. The fact that AMS's γ-ray energy threshold is an order of magnitude larger than EGRET's, thereby implying an integrated point source flux about an order of magnitude lower for AMS than for EGRET, is compensated for by the fact that AMS's angular aperture (half-angle area of 30°) is larger than EGRET's ($\sim$ 20°), and by the fact that AMS spends 100% of its time pointing to the sky (being attached to a gravity-gradient stabilized Space Station), while EGRET typically points one-third of the time to Earth. AMS lacks the low-energy end of EGRET's range due to the curvature of the electron-positron pair in AMS's magnetic field, which limits the γ-ray aperture to $\geq$ 300 MeV. On the other hand, EGRET lacks the high-energy end of AMS's range due to the effect of electromagnetic backsplash in EGRET's NaI calorimeter which vetos most events above 30 GeV.

The above table shows that AMS/γ and EGRET have very similar γ-ray detection capabilities, so that AMS will be able to continue and extend the investigation of galactic and extragalactic γ-ray sources initiated by EGRET. One main difference between the two detectors, that of significant aperture above 30 GeV for AMS/γ, may lead to the observation of new phenomena in this relatively uncharted region. A more detailed discussion of the astrophysics goals of AMS/γ, and in particular the prospect for novel discoveries, is given in the next section.

4 Gamma Ray Astrophysics Goals of AMS/γ

4.1 Blazar Astrophysics

Until the launch of CGRO, only one extragalactic source of > 0.1 GeV γ-rays was known, the blazar 3C 273, detected by the early γ-ray satellite COS-B [15]. EGRET has subsequently increased the number of detected blazars to over 50 [9], and in fact all of the extragalactic sources seen by EGRET are blazars. The term *blazar* is used to describe a wide variety of objects, such as flat-spectrum radio quasars, optically violent variable (OVV) quasars, and BL Lac objects, all of which are characterized by high luminosity and rapid time variability. Within the "unified

model" [16] these γ-ray-loud sources have a common source of energy: the accretion of matter onto a supermassive ($10^{7-10} M_{\odot}$) black hole, which in turn funnels much of its expelled energy along the black hole spin axis, forming relativistic "jets" of outflowing plasma [17]. When the axis of such a jet points towards Earth, relativistic beaming effects dramatically increase the apparent luminosity and time variability of these sources, producing a "blazar" signature [18]

Nearly all EGRET blazars are found to have their luminosity peaking in the γ-ray region, i.e., at levels higher than the radio, IR, optical, or x-ray regions [19]. Blazars detected by EGRET are found to belong to the blazar subclasses of flat-spectrum-radio-quasars and radio-selected BL Lacs [19, 20, 21], whose γ-ray emissions extend to the tens of GeV, but apparently fall off at higher energies, since they are not detected by ground-based instruments whose energy thresholds are as low as 200 GeV. Ground-based instruments, on the other hand, have detected a total of 5 blazars worldwide, all of one subclass, x-ray-selected BL Lacs. Of these 5 blazars, EGRET has detected only one (Mrk 421). Clearly an interesting transition is occurring between the effective EGRET cutoff of $\sim$ 20 GeV and the present ground-based detector threshold of $\sim$ 200 GeV, the observation of which may help determine the γ-ray production mechanisms within the blazar jets. It is not known whether the spectral cutoffs at $\sim 10^2$ GeV of EGRET blazars are due to intrinsic processes within the jets, or are due to extinction of the higher energy γ-rays off the diffuse, extragalactic soft photon (IR-optical) background [22] (via $\gamma\gamma \rightarrow e^+e^-$ interactions) as they propagate over cosmic distances to Earth.

4.1.1 Source Counts

The number of blazars that we expect to detect with AMS/γ can be estimated from the EGRET blazar population. During its first six years of operation (1991 to 1997) EGRET has claimed the detection of 51 blazars [9]. Different identification methods, however, have resulted in an EGRET blazar count ranging from 42 [23] to roughly 60 [24]. Of the 71 unidentified γ-ray sources detected by EGRET, 14 are at galactic latitudes $|b| > 30^{\circ}$ [25], making them likely blazar candidates.

Figure 10 shows the flux distribution of these sources (the identified blazars, plus the 14 high-latitude unidentified sources). In this figure the flux is the integral flux above 0.1 GeV, which is the effective energy threshold for the EGRET blazar studies, and the effective cutoff seen at $\sim 10^{-7}$

$cm^{-2}s^{-1}$ corresponds to EGRET's quoted flux sensitivity. The solid line shows the expected flux distribution of blazar γ-ray sources under the assumption that the radio and γ-ray fluxes are linearly correlated [26, 27]. The dashed vertical line is placed at the estimated flux sensitivity of AMS/γ, which is about a factor of two lower than that of EGRET. Note that we have previously defined our flux sensitivity in terms of the integral flux above 1 GeV (not 0.1 GeV), since our detector's energy threshold is effectively at 0.3 GeV. To place the "equivalent" AMS/γ sensitivity on this figure with the EGRET data, we have assumed a nominal E^{-2} differential source energy spectrum.

From the figure, it is seen that AMS/γ during its three-year mission should detect somewhere between 120 to 170 blazars, thus increasing the population statistics of these sources. This result is relatively model-independent; if we assume a spatially homogeneous population of sources in Euclidean space with no evolution, the count N versus flux S distribution follows a $N(> S) \propto S^{-3/2}$ power law, as given by the dotted line in Figure 10, independent of the population's luminosity distribution function. This curve differs only slightly from the evolution-dependent curve at the AMS/γ sensitivity.

With these increased statistics, improved γ-ray luminosity distribution functions can be determined [28, e.g.,], and compared to those at other wavelengths, particularly at the radio [29, e.g.,]. Examination of the correlation between the radio and γ-ray luminosity functions would help, for example, to discriminate between γ-ray production models which predict different beam profiles of the emitted radiation (the γ-ray intensity as a function of viewing angle from the jet axis). For example, if the photons upscattered by the synchrotron-emitting electrons are "external" photons, coming from an accretion disk, the beam profile will be substantially narrower than if the upscattered photons are the synchrotron photons [30].

4.1.2 Detection of the Extragalactic Soft Photon Background

All of the blazars detected by EGRET with high ($> 6\sigma$) significance are found to have power law spectra, $dN/dE \propto E^{-\alpha}$, where the spectral indices α range from 1.7 to 2.5, with a mean index of 2.15 [9]. The measured energies range from the EGRET threshold of 0.1 GeV up to several GeV, the value of the upper energy being statistics limited and hence a function of source strength.

Under the assumption that one can extrapolate these power law spectra to TeV energies, several EGRET blazars should be detectable with ground-based atmospheric Cerenkov telescopes. In observations of EGRET blazars by the Whipple Observatory [31], however, *no* EGRET blazars other than the BL Lac object Mrk 421 were detected. For the blazars 3C 279, 1633+382, and 2022-077, for example, the extrapolated EGRET flux is well above the sensitivity limit of the Whipple, yet these sources are not seen. Clearly something is happening to the γ-ray spectra of these blazars between a few GeV and the Whipple threshold energy (400 GeV at the time of these measurements).

Figure 11 shows the EGRET power law spectra for four blazars extrapolated to 700 GeV. It should be noted that the majority of EGRET blazars are observed to be variable sources, with time-varying γ-ray flux amplitudes and spectral indices [9]. We have somewhat arbitrary chosen a single flux amplitude and spectral index for each source from the Second Catalog [25] for purposes of illustration in Figure 11. Also shown are γ-ray flux upper limits for 1633+382 and 3C279 measured by the Whipple ACT, which are seen to be far below the extrapolated power law spectra for these sources.

There are a few possible reasons for a spectral cutoff between a few GeV and a few hundred GeV: (1) a cutoff in the electron spectrum due to synchrotron and inverse-Compton cooling may cause a corresponding cutoff in the upscattered γ-ray spectrum (an "intrinsic" cutoff mechanism) [33, e.g.,]; (2) γ-ray extinction through pair-producing interactions with the diffuse infrared (IR) to ultraviolet (UV) photons of the intergalactic photon background (IB) (an "extrinsic" cutoff mechanism) [34, 22]; and/or (3) γ-ray extinction through pair-producing interactions with photons in the local environment of the jet, produced either within the jet or from the neighboring accretion disk (an "intrinsic" cutoff mechanism).

By directly measuring the spectral cutoffs of the stronger blazar souces such as 1633+382 and 3C279, AMS/γ may determine whether these known cutoffs are due to intrinsic mechanisms, or to the extrinsic process of interaction with IB photons. The main criterion for identifying the "extrinsic" mechanism is that the cutoff energies should decrease with increasing source redshift z, since the integrated opacity of the IB increases with source distance. The opacity τ to a source

of redshift z_e at a measured γ-ray energy of E_0 is given by

$$\tau(E_0, z_e) = c \int_0^{z_e} dz \, \frac{dt}{dz} \int_0^2 dx \, \frac{x}{2} \int_0^\infty d\nu \, (1+z)^3 \frac{u_\nu(z)}{h\nu} \sigma_{\gamma\gamma}(s), \tag{9}$$

where u_ν is the differential IB energy density at frequency ν, $\sigma_{\gamma\gamma}(s)$ is the $\gamma\gamma \rightarrow e^+e^-$ cross section as a function of the center-of-mass energy $\sqrt{s}$, t is time, and $x \equiv (1 + \cos\theta)$, θ being the angle between the γ-ray and the soft photon momenta. Figure 11 shows the calculated γ-ray attenuation for two different models of the near-IR to UV intergalactic photon background [35]; one sees that the cutoff energy decreases with increasing redshift of the source. This figure also shows the "fauxdata" points of the AMS/γ spectra for these sources acquired over a two-year period of operation, under the assumption (for illustrative purposes) of power law spectra that are constant in time. These are obtained by convolving the source spectrum with the instrumental energy resolution function shown partially in Figure 9. The energy bin widths are indicated in the fauxdata for 3C273; the statistical errors are also shown at each energy point for the four sources. The effects of attentuation (according to the solid line predictions) have been included in the calculation of the fauxdata.

Cutoffs are evident in the AMS/γ spectra of the stronger sources at higher redshifts (3C279 and 1633+382), at energies ranging from 30 to 100 GeV. At higher energies the statistics are too low (and the AMS/γ energy resolution is significantly worsened) for AMS to measure blazar cutoffs. Since the threshold condition for pair production is $2E\epsilon(1 - \cos\theta) > 4m_e^2c^4$, where ϵ is the background photon energy, for a γ-ray of energy $E_{\rm TeV}$ only those background photons with energy $\epsilon_{\rm eV} > 0.3/E_{\rm TeV}$ can contribute to the opacity. Thus AMS/γ will only be able to detect γ-ray attentuation due to the IB of optical and UV photons. Therefore the observation of such a redshift-dependent cutoff would constitute a *direct*, finite measurement of the intergalactic optical and UV photon background, which has not yet been made. Conversely, the *absence* of a redshift dependence for observed blazar cutoffs would definitively point to an intrinsic cutoff mechanism in the γ-ray production in jets.

Finally, it has also been pointed out that if the IB spectrum $u_\nu(z)$ were known to high precision, then a measurement of blazar cutoffs, should they be extrinsic, would provide a measure of Hubble's constant H_0 [36], since the dt/dz term in Eq. 9 contains a factor of H_0^{-1}. Unfortunately, it is unlikely that such accurate spectral information will be available in the forseeable future in

the optical or UV bands.

4.2 Gamma Ray Bursts

Gamma ray bursts (GRBs) are likely to be the most energetic phenomena that occur in the universe. These point-source events flare into being with short, intense bursts of x-rays and γ-rays, then quickly fade away. GRBs are isotropically distributed in the sky, with no statistical evidence for repeating bursts occuring from a single source. First detected in the 1960's by the Vela satellites (whose function it was to search for nuclear weapons testing), it is only within the last two years that this class of events has been identified as being cosmological in origin, implying energy outputs on the order of 10^{51} to 10^{53} ergs released within a time scale of seconds. This rivals the mean luminosity of *the entire universe*, approximately 10^{53} erg/s [37].

One of the two most popular current models for GRBs is the merger of binary neutron stars (with a maximum energy release of 5×10^{53} ergs) or of a neutron star and black hole companion, an event which is estimated to occur on the order of once every 10^6 years per galaxy, in excellent agreement with the observed rate of GRBs (about one per day by the BATSE instrument of CGRO) [38]. The contending model is that GRBs are the results of "hypernovae", extremely energetic supernovae that result from the gravitational collapse of very massive stars.

The nonthermal x-ray and γ-ray radiation observed from GRBs is most likely produced by ultra-relativistic particles (electrons and protons) that are accelerated in the shock waves generated in the expanding fireball that follows the progenitor event. The strongest detections of GRBs are in the x-ray region of hundreds of keV, in which the BATSE, BeppoSAX, ROSAT, and ASCA orbiting instruments operate. Some of the very strongest bursts have also been detected in GeV γ-rays by EGRET (four bursts with γ-rays above 0.1 GeV), one GRB yielding photon energies up to 26 GeV [39]. Given the relatively low sensitivity of EGRET to GRBs, the detection rate by EGRET is consistent with *all* GRBs having spectra that extend to GeV energies (and possibly higher), possibly with nearly constant values of $E^2 dN/dE$ [40].

It is in fact the *highest* energy γ-rays that are the most constraining on the fireball models of GRBs; with the significantly larger sensitivity to > 10 GeV γ-rays that AMS/γ has compared to EGRET, the timing and spectral data of GRB γ-rays detected by AMS/γ could be invaluable

in elucidating the nature of the GRB fireball. Such data could also be applied to the question of whether the ultra-high energy cosmic rays might originate in the fireball shocks of GRBs [41]. The fundamental issue involves the "compactness" of the GRB fireball, which is a dimensionless ratio of source luminosity to source radius. The higher the compactness, the greater the opacity for γ-ray emission, due to the large density of lower energy photons in the fireball that are above threshold for pair production. Fireball dimensions are causally limited by x-ray timing variations, whose time constants are sometimes as low as $\sim 10^{-3}$ s. Based on distance estimates from optical measurements, the luminosity of the fireballs can be inferred. These combine to form an average optical depth for $\gamma\gamma \rightarrow e^+e^-$ of $\sim 10^{15}(E/10^{51}\text{ergs})(\delta T/10\text{ msec})^{-2}$ [38]. In spite of the enormous estimated opacities, γ-rays are observed from GRBs. This conflict can be resolved if the fireball is expanding with a very large Lorentz factor. Relativistic kinematics then both boost the γ-ray energy and observed luminosity of the source, plus reduce the time constants of timing variations, so that the apparent optical depth is approximately a factor $\Gamma^{4+2\alpha}$ larger than the actual value (α is the spectral index of the GRB spectrum). This argues for bulk Lorentz factors $> 10^2$. The higher the observed γ-ray energies, the larger the fireball Lorentz factor must be to allow these γ-rays to escape the fireball region [42].

In addition, there is a relationship between the redshift of a given GRB and the maximum energy γ-ray that can be received at Earth, due to the effect of extinction via pair production off the cosmic optical and UV photon background (see Sec.4.1.2). No photons with energies above 20 GeV, for example, have been detected from sources *known* to have redshifts above unity. Detection by AMS/γ of any γ-ray energies above ~ 20 GeV, coupled with an independent lower limit to the redshift of the GRB source via optical measurements, would place limits on the energy densities of the cosmic photon backgrounds if the redshift were on the order of unity or greater.

The time distribution of the γ-ray events, relative to the prompt x-ray bursts that are observed, is also of great importance. In one GRB, GeV γ-rays were observed by EGRET *for over one hour* after the initial x-ray burst [39]. A number of scenarios have been proposed to explain this delayed emission, ranging from generation in more distant (external) shocks by the fireball, to the deflection of e^+e^- pairs in the intergalactic magnetic field, followed by inverse Compton scattering that produces the γ-rays [43].

It is not possible to predict with certainty how many GRBs will be detected by AMS/γ. Given the comparable total exposures ($> 10^{11}$ cm^2-s-sr for AMS) of EGRET and AMS/γ over the lifetimes of the two instruments, one could use the limited statistics of EGRET's four GeV GRBs as a naive estimate. In fact, it is likely that fewer would be detected by AMS/γ due to the higher effective energy threshold of 0.3 GeV for AMS/γ, compared to 30 MeV for EGRET. A GRB similar to the one strong burst observed by EGRET, GRB940217 [39], would certainly be detected by AMS/γ if the burst were within a few tens of degrees from the orbital plane of the Space Station. Since the FOV of EGRET is smaller than that of AMS/γ, and since EGRET was not targeting GRB940217 when it occurred, it is safe to say that the *a priori* detection probability of a strong GeV burst by AMS/γ would be larger than for EGRET.

4.3 The Extragalactic Gamma Ray Background at High Energies

EGRET has recently measured the spectrum of the isotropic extragalactic γ-ray background (EGRB) [10], as shown in Figure 12. Originally detected by the SAS-2 satellite telescope at energies above 100 MeV [44], the origin of this background is still uncertain, and may be due to diffuse processes such as secondary production from cosmic ray collisions with intergalactic gas [45, 46], or, more likely, the accumulated emission of unresolved point sources, such as blazars or other classes of active galactic nuclei [47, 48].

4.3.1 The Role of Blazars

In particular, the hypothesis that unresolved γ-ray blazars are responsible for the EGRB has been examined, with conflicting conclusions [26, 28]. Stecker and Salamon (1996), by assuming a linear relation between the radio and γ-ray luminosity functions of blazars [27], fit EGRET's blazar flux distribution (see Section 4.1.1), and also predicted the unresolved blazar contribution to the EGRB, shown in Figure 12. They were able to account for 100% of the observed EGRB, but predicted a sharp cutoff near 20-40 GeV due to the effects of γ-ray extinction off the IB optical and UV photons [32]. A more recent estimate of the γ-ray luminosity function of blazars, however, finds that unresolved blazars contribute only 25% of the total EGRB, thus indicating the need for additional (nonblazar) sources. Such a conclusion would not be inconsistent with an

EGRB whose spectrum continues as a power law to energies above 100 GeV.

Whether blazars can or cannot contribute 100% of the EGRB may be resolved with the increased statistics at the highest energies that AMS/γ will obtain. If EGRET-type blazars do contribute 100% of the EGRB, then a cutoff *must* be present somewhere below 100 GeV. Although the latest EGRET data shows no evidence of a cutoff in the EGRB spectrum, and is consistent with a pure power law (Eq.5) [10], EGRET's systematic errors make the current data somewhat inconclusive. AMS/γ in two years of operation should detect $\sim 10^5$ EGRB γ-rays in the interval 0.5-1.0 GeV, and $\sim 10^3$ between 50-100 GeV; assuming that systematics can be kept to the several percent level, a spectral cutoff occurring within the 20-40 GeV region would be detectable by AMS/γ.

4.3.2 Instrumental Backgrounds to the EGRB Measurement

Any measurement of the EGRB requires that instrumental background events be kept to a lower rate than the EGRB flux. To estimate the effects of background due to collisions of cosmic ray electrons, positrons, and protons with the AMS instrument, we divided the γ-ray spectrum into four bins per decade of energy (from 0.5 to 100 GeV) and required that we investigate backgrounds down to a level of 20% of the EGRB rate in *each* energy bin. For example, in the 25-40 GeV bin it will take AMS/γ 2.0×10^5 seconds to obtain 5 EGRB γ-rays. In our Monte Carlo analysis, therefore, we threw 2.0×10^5 seconds' worth of cosmic ray electron, positron, and proton flux at the instrument to generate a false γ-ray background. These cosmic rays were thrown isotropically over a zenith angle range of $0^\circ < \theta < 110^\circ$, where the largest zenith angle corresponds to the location of the Earth limb at an orbital altitude of 400 km. The energies were distributed according to known electron, positron, and proton energy spectra as discussed below.

For cosmic ray electrons above 10 GeV, we used the compiled data presented in Müller and Tang (1987) [49] to estimate the electron spectrum, and for energies below 10 GeV we used the data of Golden et al. (1994) [50]. We note that this latter set of data was obtained by a balloon flight in northeastern Canada, where the geomagnetic rigidity cutoff is well below 1 GV; since AMS during most of its orbit will be in regions with much higher rigidity cutoff (up to 15 GV near the equator), the use of the Golden etal data for the low energy electron spectrum is quite

conservative. Approximately 10^7 electrons in all were thrown at the AMS instrument, of which 0.1% met the basic reconstruction criteria for a γ-ray candidate event. Additional quality cuts were applied so that this background was reduced to at most one count per energy bin (for a total of 2 background events). These cuts were then applied to the actual γ-ray data as described in Section 3.1. The positron flux was assumed to be 0.1 times that of the electron flux over the full spectrum (measurements give this ratio as varying between 0.05 to ~ 0.2 above 0.5 GeV [51]). For a given γ-ray energy bin $[E_{\rm low}, E_{\rm high}]$, only electrons and positrons of energies greater than $E_{\rm low}$ were considered to be potential sources of γ-ray background. This assumption, justified by the fact that none of the reconstructed background events had energies higher than their progenitor electrons or positrons, reduced computational demands significantly.

For cosmic ray protons we used the recent absolute flux measurements of Menn etal (1997) [52] which were obtained in a balloon flight at low geomagnetic cutoff. As with the electrons, therefore, our estimated low energy proton flux is conservatively high. Unlike electrons, which can generate bremsstrahlung photons with nearly the full primary electron energy, protons collisions generate γ-rays primarily through π^0 decays (direct γ-ray production is only at the level of 10% that of π^0s at 500 GeV/c, for example [53]), where the secondary π^0s carry only a fraction of the primary proton energy. Therefore, even though the CR p/e ratio is $\sim 10^2$, we do not need to follow 10^9 protons (compared to 10^7 electrons) through the detector. Instead, when estimating background production for the γ-ray energy bin $[E_{\rm low}, E_{\rm high}]$, only protons of energy $> \eta E_{\rm low}$, $\eta > 1$, were considered. We chose the value $\eta = 7$ based on calculations of galactic γ-ray production via CR proton interactions with the interstellar medium by Mori [54]. Using the HADRIN, FRITIOF, and PYTHIA particle collision codes, and convolving with the CR proton spectrum, Mori found that for a fixed γ-ray energy E_γ roughly half the photons were produced by protons of energy $> 7E_\gamma$. This reduced our computational load by $\sim \eta^{-1.7}$ given the integral proton spectrum of $E^{-1.7}$ above a few GeV; approximately 3×10^7 protons were required for these studies. We found that with the quality cuts introduced to eliminate the electron-induced background events, we had at most one proton-induced background γ-ray per source-energy bin (for a total of 5 background events); all these had reconstructed energies of < 1 GeV.

4.4 Detection of Neutralino Annihilation

It is well known that the luminous matter within galaxies, and within our Galaxy in particular, is far below that required to explain the gravitational dynamics of their components. The inability of the estimated mass from disk and gas components to account for the observed rotation curves of spiral galaxies, for example, is exemplified in Figure 13, implying the presence of a "dark matter" component whose density falls off roughly as r^{-2}, where r is the distance from the center of the galaxy. Although MACHOs (massive compact halo objects) may possibly account for a significant fraction (20% to 100%) of the inferred dark matter in our Galaxy [55, 56], the role of MACHOs in the mass budget of the Galaxy is still very poorly defined, and may prove to be minor [57]. An alternative is that this dark component is comprised of WIMPs (weakly interacting massive particles), one candidate for which is the supersymmetric neutralino, χ. (The subject of supersymmetric dark matter has recently been comprehensively reviewed by Jungman, Kamionkowski, and Griest (1996)[58].)

Should supersymmetric neutralinos be the dominant dark matter component, the mutual annihilation of these Majorana particles near the center of the galaxy would produce a number of signatures, one of which would be the emission of both line and continuum γ-rays whose characteristic spectra would distinguish them from other contributions to the diffuse γ-ray background. The flux of monochromatic (line) γ-rays per solid angle from $\chi\chi \rightarrow \gamma\gamma$ or $\chi\chi \rightarrow Z\gamma$ annihilations in the galactic halo is given by [59]

$$\frac{dF}{d\Omega} = \eta_\gamma \frac{\langle \sigma_{\chi\chi} v \rangle}{8\pi M_\chi^2} \int_0^\infty \rho_\chi^2(l,\psi)\, dl(\psi), \tag{10}$$

where ρ_χ is the neutralino mass density, M_χ is the neutralino mass, $\sigma_{\chi\chi}$ is the annihilation cross section into $\gamma\gamma$ or $Z^0\gamma$, the leading factor $\eta_\gamma = 2$ for $\chi\chi \rightarrow \gamma\gamma$ and $\eta_\gamma = 1$ for $\chi\chi \rightarrow Z\gamma$, ψ is the angle between the viewing direction and the direction to the center of the Galaxy, and l is the distance along the viewing direction. Because the annihilating particles are identical, the production rate per unit volume is $\eta_\gamma (n_\chi^2/2)\, \langle \sigma_{\chi\chi} v \rangle$, where the factor of 1/2 in $n_\chi^2/2$ eliminates double-counting of annihilating pairs. Equation 10 can be expressed in the form

$$\frac{dF}{d\Omega} = \left[3.16 \times 10^{-11} \mathrm{cm}^{-2}\mathrm{s}^{-1}\mathrm{sr}^{-1}\right] \left[\frac{\eta_\gamma}{2}\right] \left[\frac{\langle \sigma_{\chi\chi\rightarrow\gamma\gamma} v \rangle}{10^{-29}\mathrm{cm}^3\mathrm{s}^{-1}}\right] \left[\frac{10\mathrm{GeV}}{M_\chi}\right]^2 \left[\frac{\rho_0}{0.4\mathrm{GeV/cm}^3}\right]^2 \left[\frac{R_0}{8.0\mathrm{kpc}}\right] J(\psi), \tag{11}$$

where

$$J(\psi) \equiv \int_0^\infty \frac{\rho_\chi^2}{\rho_0^2}\, d\left(\frac{l}{R_0}\right)(\psi). \tag{12}$$

Estimates of the distance of the Sun to the Galactic center, R_0, vary from 6 to 10 kpc, with a weighted mean of 8.0 ± 0.5 [60] (to be compared with the "standard" value of 8.5 kpc adopted by the IAU in 1985 [61]). We take $R_0 = 8.0$ kpc. The local dark matter density ρ_0 is obtained from measurements of the circular rotation velocity $v_c(R)$ of our Galaxy, where R is the galactocentric radius. The contributions to $v_c(R)$ from the disk and bulge (baryonic) components are subtracted, leaving a residual of $v_{c,halo}(R)^2 \approx GM(R)/R$. Fitting this to various dark matter halo profiles then yields the parameter ρ_0. This has been done recently by Dehnen and Binney [62], who obtain values of ρ_0 ranging from 0.1 to 0.7 GeV/cm^3, depending on the assumed halo density profile. These authors also conclude that the mass distribution of the Galaxy is currently ill-determined, so no one model is clearly preferable over others.

The form of the halo density profile $\rho(R)$ is critical to the question of observability of γ-rays from neutralino annihilation. The simplest assumption, that of an isothermal halo, leads to a density profile ρ which is constant for $R \ll a$, where a is the "core" radius, and which falls as r^{-2} for $R \gg a$ [63], accounting for the flat rotation curves of spirals at large radii. High resolution, N-body numerical simulations of the collapse of cold dark matter (CDM) halos, however, show no signs of the existence of a halo "core" down to the smallest resolvable scales. Studies by Navarro, Frenk, and White (NFW) (1996,1997)[64, 65], corroborated by others [66], show that CDM halos over a wide range of total mass obey a "universal" density profile, given by

$$\rho(R) \propto \frac{1}{R(1+R/a)^2}, \tag{13}$$

where a is a scale radius. Although this profile results in a singular annihilation rate at the galactic center, the total γ-ray flux over any finite solid angle about $\psi = 0$ is finite. Even steeper radial dependences have been proposed: Berezinsky, Gurevich, and Zybin (1992)[67] argue theoretically for $\rho(R) \propto R^{-1.8}$ down to a cutoff of $R \sim 1$ pc, but this result has been criticized as arising from their use of unphysical initial conditions [68]. However, in the mass modelling of the Galaxy by Dehnen and Binney [62], one of their models has an $R^{-1.8}$ density profile down to a core radius of $a = 1$ kpc, and fits the dynamical data with a good χ^2. Recent analyses of dwarf and low-surface

brightness galaxies, whose dark matter fraction may reach levels of 95%, indicate the presence of central cusps with density profiles $\rho(R) \propto 1/R^{\gamma},\ \gamma \approx 0.2 - 0.4$ [69], significantly shallower than that of NFW. It is not clear, however, that these shallower cusps are present in larger galaxies, such as our Galaxy, since the cusp steepness may depend on how dynamically "relaxed" the halo has become [69].

To estimate the potential sensitivity of AMS to monochromatic photons from neutralino annihilation, we use three of the halo profiles determined by Dehnen and Binney, corresponding to their models 2d, 4d, and 2f, plus a generic quasi-isothermal profile. All the Dehnen and Binney halo profiles take the form

$$\rho(\varrho) = \rho_a \left(\frac{\varrho}{a}\right)^{-\gamma_h} \left(1 + \frac{\varrho}{a}\right)^{\gamma_h - \beta_h}, \tag{14}$$

where $\varrho = (R^2 + z^2/q^2)^{1/2}$, R being the radial distance along the plane of the galaxy, z being the height above the plane, and $q = 0.8$ being the assumed oblateness of the halo. The halo profile exponents γ_h and β_h vary with the mass model, and are given in table below:

model	γ_h	β_h	a (kpc)	ρ_a ($M_\odot$/pc^3)	ρ_0 (GeV/cm^3)
D&B 2d	1	3	21.8	0.006159	0.34
D&B 4d	1	3	5.236	0.1101	0.43
D&B 2f	1.8	1.888	1.0	0.4179	0.31
isotherm			1.0		0.30

In models 2d and 4d, the density profile is fixed to follow the "universal" profile found by NFW, for which $\gamma_h = 1$ and $\beta_h = 3$. The last halo profile is an approximation to the true isothermal profile (see Binney & Tremaine, 1987):

$$\rho(R) = \rho_0 \left(\frac{a^2 + R_0^2}{a^2 + R^2}\right). \tag{15}$$

Figure 14 shows the resulting $J(\psi)$ curves for the various halo profiles.

The remaining two parameters that determine the γ-ray flux are, from Eq. 11, the neutralino mass M_χ and the annihilation cross sections $\sigma_{\chi\chi}$ that result in γ-ray production. Monochromatic photons from $\chi\chi \to \gamma\gamma$ and $\chi\chi \to Z^0\gamma$ are necessarily produced via box diagrams [70, 71], and so have a smaller branching ratio that tree-level annihilation into W and Z^0 pairs. Secondary γ-rays from the decay of tree-level W's and Z^0's give a much larger continuum flux, which, depending on

the SUSY parameters, may be well above the extragalactic γ-ray background flux (Section 4.3) near the Galactic center [74].

4.4.1 AMS Sensitivity to Monochromatic Gamma Rays from Neutralino Annihilation

Monochromatic γ-ray detection is limited both by detector energy resolution (Fig. 9) and aperture. Should the expected event rate be significantly greater than unity, the line width must be small enough so that the signal is not lost in the galactic and extragalactic γ-ray backgrounds. The rapid deterioration of energy resolution above 100 GeV limits AMS detection of *monochromatic* γ-rays to neutralino masses $M_\chi < 200$ GeV. (This limit does not apply to detection of continuum photons from W and Z^0 decays; see Section 4.4.2.) However, recent analysis by the DAMA/NaI Collaboration has confirmed the presence of an annual modulation in their detector's event rate (at 98.5% C.L.), suggesting the existence of a local WIMP density with a 1σ mass range $M_\chi = 59^{+22}_{-14}$ GeV, and WIMP-nucleon scalar elastic cross section $\xi\sigma^{(\mathrm{nucleon})}_{\mathrm{scalar}} = 7.0^{+0.4}_{-1.7} \times 10^{-9}$ nb, where ξ is the fraction of the local dark matter density that is due to WIMP neutralinos [72]. Within this mass range our rms energy resolution is flat at 24%. These mass and cross section ranges have also been shown to be fully compatible with a MSSM neutralino being the major component of dark matter in the universe [73].

Figure 15 illustrates the sensitivity of AMS to detection of line photons from the annihilation channel $\chi\chi \rightarrow \gamma\gamma$ as a function of halo model. Plotted are integrated γ-ray counts $N(< \psi)$ as a function of angle ψ from the Galactic center for the four halo profile models, accumulated over a two-year period by AMS, assuming $M_\chi = 50$ GeV and a velocity-cross section product $v\sigma = 10^{-29}$ cm^3/s. With an energy acceptance width of 20 GeV, approximately 80% of the line photons are captured. The dot-dashed line shows the galactic and extragalactic background count for this energy window; the parameterization of Bergström, Ullio, and Buckley [74] was used for the galactic background contribution. The dashed and dotted lines correspond respectively to the "Berezinsky-like" halo (model 2f of Dehnen and Binney [62]) and the quasi-isothermal halo, while the upper and lower solid lines correspond to models 4d and 2d of Dehnen and Binney, which are the NFW-like models.

Bergström and Ullio [71] have recently performed a full one-loop calculation of the $\chi\chi \to \gamma\gamma$ annihilation reaction, assuming the minimal supersymmetric extension of the standard model (MSSM). They performed extensive scans in SUSY parameter space to map out the range of values of the annihilation cross section versus neutralino mass. We have reproduced their Figure 3a in Figure 16, along with the AMS sensitivity for the two most optimistic halo profiles, models 2f and 4d, expressed as a lower limit on $\langle v\sigma \rangle$ versus M_χ for detection of neutralino annihilation. The detection criteria were arbitrarily chosen to be $N_\gamma \geq 10$ and $N_\gamma/\sqrt{B_\gamma} \geq 6$, where N_γ is the total number of annihilation γ-rays detected over a 2-year operating period within the central few degrees of the Galactic Center, and B_γ is the total number of background photons from diffuse galactic emission detected within the energy window and the same solid angle about the Galactic Center.

Ullio and Bergström [70] also performed a MSSM full one-loop calculation of neutralino annihilation via $\chi\chi \to \gamma Z$, assuming a pure higgsino state for the neutralino. For this channel the γ-ray has an energy $E_\gamma = M_\chi - m_Z^2/4M_\chi$. In Figure 17 we have reproduced Figure 6 of Ullio and Bergström, which shows their $v\sigma_{Z\gamma}$ versus higgsino mass (solid line), along with the unitary lower bound on this cross section (dashed line). Superimposed on this plot is a line segment which shows the minimum $v\sigma_{Z\gamma}$ required for detectability by AMS over a 2-year period, assuming the "Berezinsky-like" halo model 2f of Dehnen and Binney [62]. None of the other halo models intersect the Ullio and Bergström curves. Thus for this pure higgsino annihilation channel only the most singular halo profile can yield a detectable signal.

In general, then, only the more singular of the halo profile models, in which the dark matter density continues to increase as $R^{-\gamma}$, $\gamma \sim 1-2$, can give hope for line photon detection by AMS, and then only in a restricted region of MSSM parameter space. It should be kept in mind that a fraction of this restricted region may already have been eliminated by the absence of a detection by EGRET, but such an analysis has yet to be completed [75].

4.4.2 AMS Sensitivity to Continuum Gamma Rays from Neutralino Annihilation

Continuum photons from the decay of Ws and Zs produced by tree-level annihilations $\chi\chi \to WW, ZZ$ are far more abundant than the line γ-rays considered above, and so possibly provide

the greatest chance for detection, assuming the neutralino mass is above that of the W and Z. Berström, Ullio, and Buckley [74] have used the PYTHIA Monte Carlo code [76] to determine the the continuum photon energy distribution from $\chi\chi$ annihilation into WW, ZZ, and $q\bar{q}$ pairs. They find that the hardest distributions come from WW and ZZ pairs, and that the annihilation rate is dominated by WW and ZZ production at higher (higgsino-like) neutralino masses. From a scan of MSSM parameter space, they find that the models with the highest rate of WW and ZZ production yield an observed differential photon flux of

$$\frac{dF_\gamma}{dE_\gamma} \approx 1.2 \times 10^{-10} \left(\frac{300 \text{ GeV}}{M_\chi} \right)^4 \frac{dN_\gamma}{dE_\gamma} J(\psi) \ \ \text{cm}^{-2}\text{s}^{-1}\text{sr}^{-1}\text{GeV}^{-1}, \tag{16}$$

where

$$\frac{dN_\gamma}{dx} = M_\chi \frac{dN_\gamma}{dE_\gamma} = \frac{0.73}{x^{1.5}} e^{-7.8x}, \tag{17}$$

for $M_\chi > 300$ GeV. The $J(\psi)$ factor is given by Eq. 12.

Using the $J(\psi)$ functions of the four halo models described above (Fig. 14), the differential flux coming from a solid angle Ω about the Galactic Center can be obtained and compared to the flux from the galactic and extragalactic backgrounds. Using the collection area*time product $At(E_\gamma, \delta)$ (Fig. 6) for AMS, the differential event count is obtained. Figures 18 to 20 show these event counts after integration over ψ out to three different solid angles about the Galactic Center, $\Omega = 10^{-3}$, $10^{-1.5}$, and 1.0 steradians. The dot-dashed line is the diffuse galactic and extragalactic background photon count; the upper and lower solid lines correspond to halos for models 4d and 2d, respectively; the dashed line corresponds to the "Berezinsky-like" halo model 2f; and the dotted line comes from the quasi-isothermal halo model. The faux-data points shown in the figures take into account the effect of detector energy resolution; these are the counts obtained in each energy bin after convolution with the Monte Carlo energy resolution functions (Fig. 8).

There are a number of salient features, the primary one being the strength of the signal compared to the diffuse background for essentially all of the halo models considered. For this particular (optimized) MSSM model it is likely that EGRET would have already provided a detection given any of the halo models considered here. Although there is a large variation in signal between the various halo models, it appears nevertheless that for *any* of these halo models a substantial region of MSSM parameter space can be constrained by the absence of a continuum γ-ray signal.

These figures also show that the differing angular dependences of the background and signal result in there being an optimal solid angle Ω that maximizes signal to noise, with more singular profiles having a stronger signal to noise at smaller solid angles. These differing angular dependences can also be used to discriminate the signal from the diffuse backgrounds.

Finally, we point out that continuum photons result from $\chi\chi \to b\bar{b}$ as well as from WW and ZZ pair production, producing scaled spectra similar to those from W and Z decays. This implies that AMS/γ sensitivity to continuum γ-rays may extend down to the current LEP limits on the neutralino mass [77].

5 Conclusions

We have shown that with minor modifications the Alpha Magnetic Spectrometer can become a powerful γ-ray detector as well, with overall performance characteristics being comparable, if not superior, to those of EGRET. With γ-ray energy resolution extending past 100 GeV, and with an aperture that is nearly flat above ~ 3 GeV, AMS/γ can address a number of outstanding issues in γ-ray astrophysics that relate to the relatively unexplored region of $E_\gamma = 20 - 200$ GeV. For one, AMS/γ will likely confirm or refute the hypothesis that unresolved blazars are responsible for the bulk of the extragalactic γ-ray background; AMS/γ will also extend the spectrum of the diffuse galactic background to above 100 GeV, helping to resolve current difficulties in interpreting the EGRET diffuse galactic background measurement [78].

AMS/γ should roughly double the total number of blazars detected in γ-rays, and will be enable multiwavelength observational campaigns to include the GeV region of blazar spectra during the flight years of 2003-2006. There is an additional possibility that an indirect detection of the cosmic UV and optical photon background can be made through the detection of extinctions in high-redshift blazars above ~ 20 GeV. AMS/γ will also likely observe GeV γ-ray emission from one or more gamma ray bursts during its operational lifetime.

AMS/γ will also search for both line and continuum emission of γ-rays from the region of the Galactic Center created by the annihilation of dark matter neutralinos. Although the sensitivity to line emission appears marginal, there is nevertheless a finite, though small, region of halo/MSSM phase space which allows a detection by AMS. However, a much larger region of dark-matter

halo/MSSM parameter space can be constrained in a search for continuum γ-rays by AMS/γ.

Finally, we note that even higher sensitivities can be reached with the addition of a high granularity calorimeter below the magnet (option (b)); this will be the subject of future work.

Acknowledgements

We thank B. Dingus, S. Hunter, and P. Ullio for helpful conversations, and P. Sreekumar for the same and for supplying us with additional, unpublished information on the EGRET measurement of the extragalactic γ-ray background. We also thank the many members of the AMS Collaboration who have indirectly contributed to this paper, and especially S.C.C. Ting for his critical comments.

References

[1] J.D. Kurfess, D.L. Bertsch, G.J. Fishman, and V. Schöfelder (1997) AIP Conf. Proc. 410, 509.

[2] D. Engovatov et al. (1997) IEEE Nucl. Sci. Symp. (Albuquerque).

[3] AGILE, Phase A Report, ASI Small Program Scientific Mission, October 1998, AR.DAS.98.501.

[4] A.M. Hillas and J.R. Patterson (1990) J. Phys. G Nucl. Part. Phys. 16, 1271.

[5] M. Acciarri et al. (1995) Nucl. Instr. Meth. A360, 103; R. Battiston (1995) Nucl. Phys. B Proc. Suppl. 44, 274.

[6] S. Ahlen et al. (1994) Nucl. Instr. Meth. A350, 351.

[7] G. Ambrosi et al. (1998), submitted to Nucl. Instr. Meth.

[8] H. Wind (1974) Nucl. Instr. Meth. 115, 431.

[9] R. Mukherjee, *et al.* (1997) Ap.J. 490, 116.

[10] P. Sreekumar, *et al.* (1998) Ap.J. 494, 523.

[11] S.D. Hunter, *et al.* (1997) Ap.J. 481, 205.

[12] D.J. Thompson, *et al.* (1993) Ap.J.Suppl. 86, 629.

[13] Jim Scheib (NASA/JSC) (1995), personal communication.

[14] T.P. Li and Y.Q. Ma (1983) Ap.J. 272, 317.

[15] B.N. Swanenberg, *et al.* (1978) Nature 275, 298.

[16] G. Ghisellini, *et al.* (1998) astro-ph/980731.

[17] G. Henri and G. Pelletier (1991) Ap.J. 383, L7.

[18] R.D. Blandford and A. Königl (1979) Ap.J. 232, 34.

[19] C. von Montigny, *et al.* (1995) Ap.J. 440, 525.

[20] R. Sambruna, L. Maraschi, and C.M. Urry (1996) Ap.J. 463, 444.

[21] F.W. Stecker, O.C. De Jager, and M.H. Salamon (1996) Ap. J. 473, L75.

[22] F.W. Stecker, O.C. De Jager, and M.H. Salamon (1992) Ap.J. 390, L49.

[23] J.R. Mattox, *et al.* (1997) Ap.J. 481, 95.

[24] [R.C. Hartman, W. Collmar, C. von Montigny, and C.D. Dermer (1997) AIP Conf. Proc. 410, 307.

[25] D.J. Thompson, *et al.* (1995) Ap.J.Suppl. 101, 259.

[26] F.W. Stecker and M.H. Salamon (1996) Ap.J. 464, 600.

[27] P. Padovani, G. Ghisellini, A.C. Fabian, and A. Celotti (1993) MNRAS 260, L21.

[28] J. Chiang and R. Mukherjee (1998) Ap.J. 496, 752.

[29] J.S. Dunlop and J.A. Peacock (1990) MNRAS 247, 19.

[30] C.D. Dermer (1995) Ap.J. 446, L86.

[31] A.D. Kerrick, *et al.* (1995) Ap.J. 452, 588.

[32] M.H. Salamon and F.W. Stecker (1998) Ap.J. 493, 547.

[33] M. Sikora, M.C. Begelman, and M.J. Rees (1994) Ap.J. 421, 153.

[34] R.J. Gould and G.P. Schreder (1966) Phys. Rev. Lett. 16, 252.

[35] M.H. Salamon and F.W. Stecker (1997) Ap.J. 493, 547.

[36] M.H. Salamon, F.W. Stecker, and O.C. De Jager (1994) Ap.J. 423, L1.

[37] K. Hurley (1998) astro-ph/9812052.

[38] T. Piran (1998) astro-ph/9801001.

[39] K. Hurley et al. (1994) Nature 372, 652.

[40] B. Dingus et al. (1997) in *Proc. 4th Huntsville Symposium on GRBs.*

[41] E. Waxman (1995) Ap.J. 452, L1.

[42] M.G. Baring and A.K. Harding (1997) Ap.J. 491, 663.

[43] R. Plaga (1995) Nature 374, 430.

[44] D.J. Thompson and C.E. Fichtel (1982) A&A 109, 352.

[45] A. Dar and N Shariv (1995) Phys. Rev. Lett. 75, 3052.

[46] F.W. Stecker and M.H. Salamon (1996) Phys. Rev. Lett. 76, 3878.

[47] G.F. Bignami, C.E. Fichtel, R.C. Hartman, and D.J. Thompson (1979) Ap.J. 232, 649.

[48] D. Kazanas and J.P. Protheroe (1983) Nature 302, 228.

[49] D. Müller and K.K. Tang (1987) Ap.J. 312, 183.

[50] R.L. Golden, *et al.* (1994) Ap.J. 436, 769.

[51] S.W. Barwick, *et al.* (1997) Ap.J. 482, L191.

[52] W. Menn, *et al.* (1997) 25th ICRC 3, 409 (Dublin).

[53] G. Alverson, *et al.* (1993) Phys. Rev. D48, 5.

[54] M. Mori (1997) Ap.J. 478, 225.

[55] C. Alcock *et al.* (1997) Ap.J. 486, 697.

[56] W. Sutherland (1998) astro-ph/9811185.

[57] M. Fukugita, C.J. Hogan, and P.J.E. Peebles (1998) Ap.J. 503, 518.

[58] G. Jungman, M. Kamionkowski, and K. Griest (1996) Phys. Rep. 267, 195.

[59] M.S. Turner (1986) Phys. Rev. D34, 1921.

[60] M.J. Reid (1993) Ann. Rev. Astron. Astroph. 31, 345.

[61] M. Fich and S. Tremaine (1991) Ann. Rev. Astron. Astroph. 29, 409.

[62] W. Dehnen and J. Binney (1996) astro-ph/9612059.

[63] J. Binney and S. Tremaine (1987) *Galactic Dynamics* (Princeton).

[64] J.F. Navarro, C.S. Frenk, and S.D.M. White (1996) Ap.J. 462, 563.

[65] J.F. Navarro, C.S. Frenk, and S.D.M. White (1997) Ap.J. 490, 493.

[66] S. Cole and C. Lacey (1995) astro-ph/9510147.

[67] V.S. Berezinsky, A.V. Gurevich, and K.P. Zybin (1992) Phys. Lett. B294, 221.

[68] R.A. Flores and J.R. Primack (1994) Ap.J. 427, L1.

[69] A.V.Kratsov, A.A. Klypin, J.S. Bullock, and J.R. Primack (1998) Ap.J. 502, 48.

[70] P. Ullio and L. Bergström (1997) hep-ph/9707333.

[71] L. Bergström and P. Ullio (1997) hep-ph/9706232.

[72] R. Bernabei et al. (1998) Roma II University preprints ROMA2F/98/27 and ROMA2F/98/34.

[73] A. Bottino, F. Donato, N. Fornengo, and S. Scopel (1998) hep-ph/9808456.

[74] L. Bergström, P. Ullio, and J.H. Buckley (1997) astro-ph/9712318.

[75] B.L. Dingus and M.H. Salamon (1998) in preparation.

[76] T. Sjöstrand (1994) Comp. Phys. Comm. 82, 74.

[77] M. Biasini (1999) in Proc. XIII Rencontres de Physique (La Thuile).

[78] M. Pohl and J.A. Esposito (1998) Ap. J. 507, 327.

[79] R. Battiston (1999) in Proc. XIII Rencontres de Physique (La Thuile); also as astro-ph/9907152.

[80] K.G. Begeman, A.H. Broeils, and R.H. Sanders (1991) MNRAS 249, 523.

[81] E.D. Bloom (1996) Sp. Sci. Rev. 75, 109.

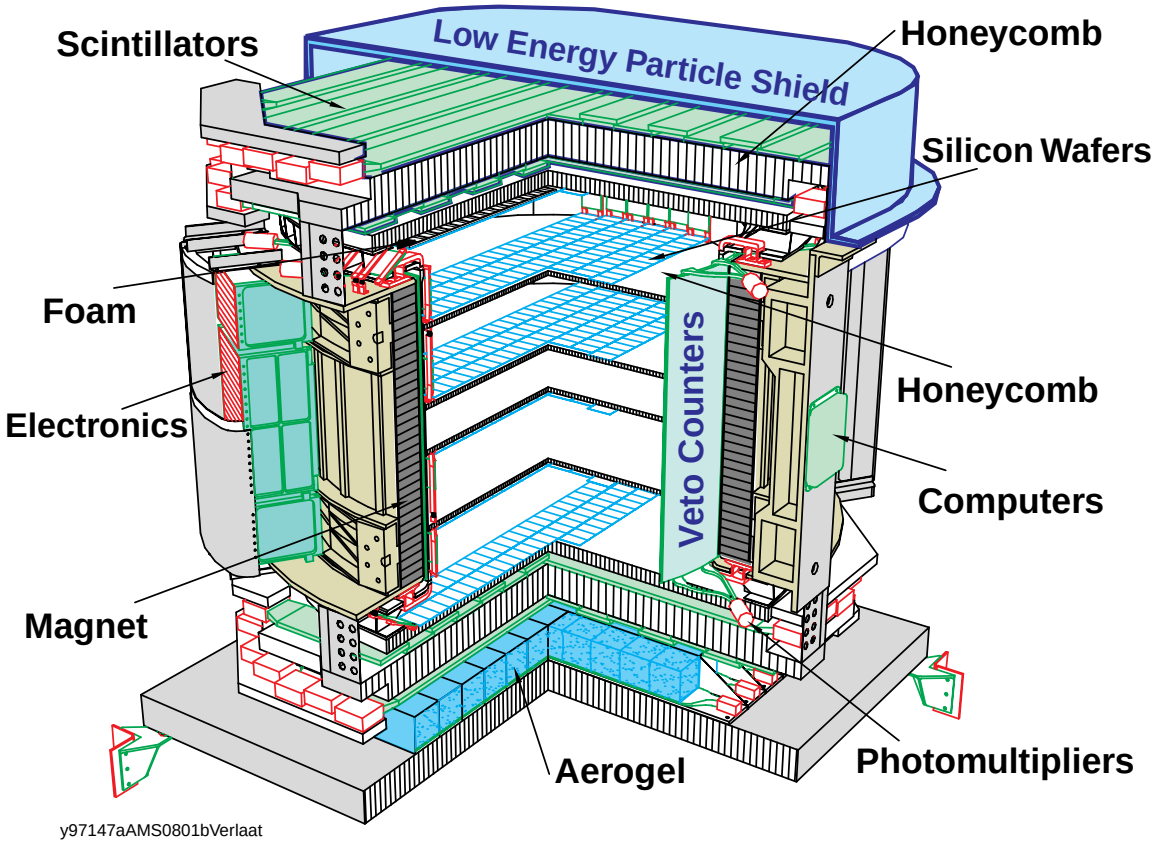

Figure 1: A cross section of the AMS instrument.

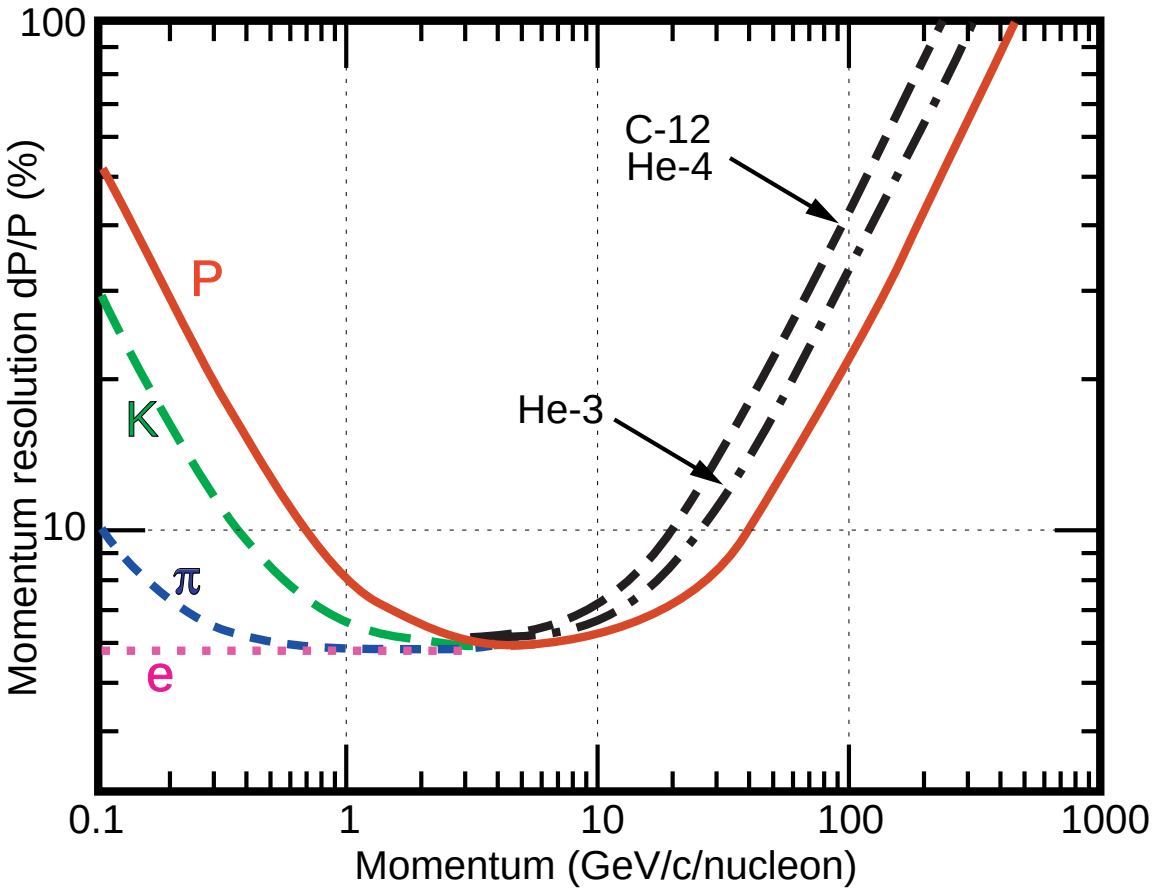

Figure 2: The momentum resolution of the AMS spectrometer for e, π, K, p, ^{3}He, ^{4}He, and ^{12}C.

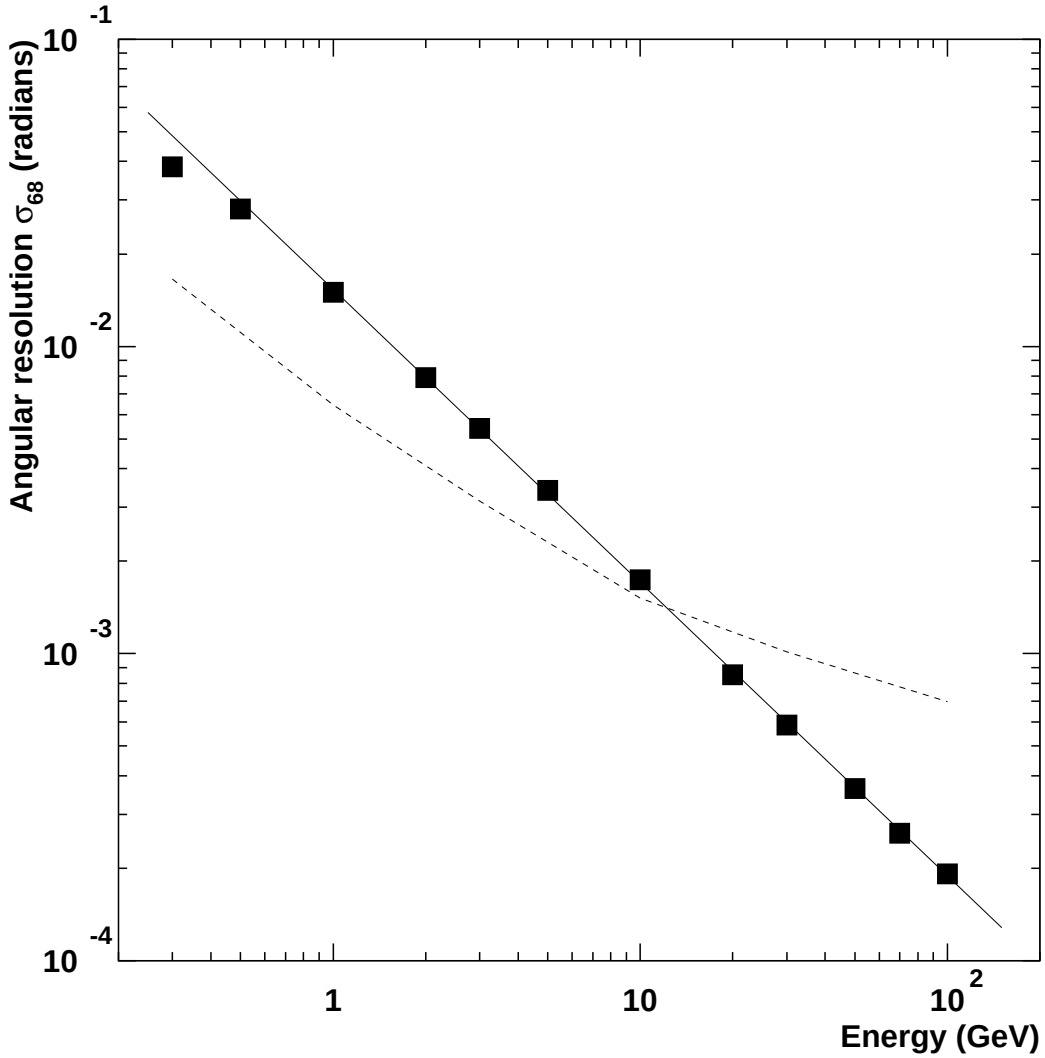

Figure 3: Angular resolution of AMS/γ as a function of primary γ-ray energy (filled squares), and that of GLAST [81] (dashed line) in the energy interval 0.3 to 100 GeV.

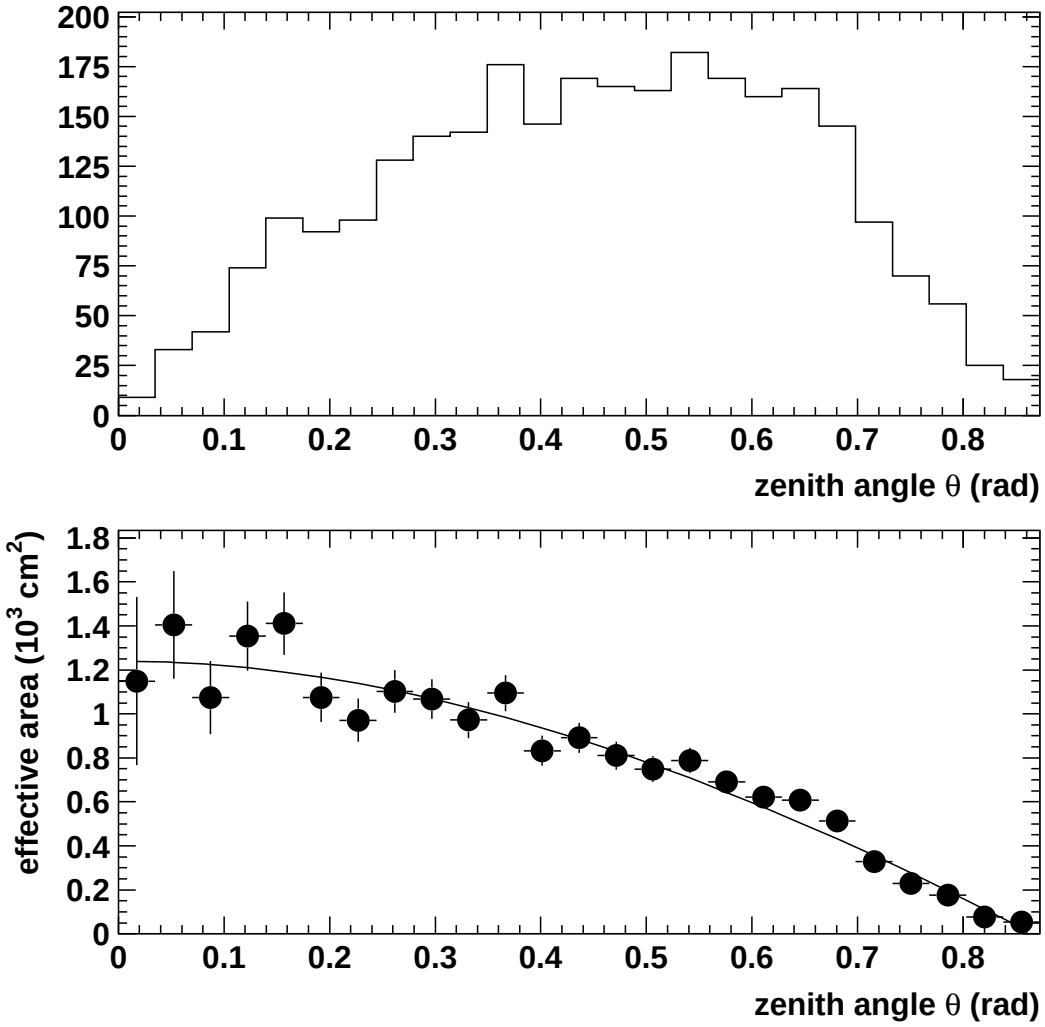

Figure 4: (a) Histogram of detected γ-rays as a function of incident zenith angle θ for 10 GeV γ-rays. (b) Effective γ-ray detection area $A(E, \theta)$ versus zenith angle at 10 GeV.

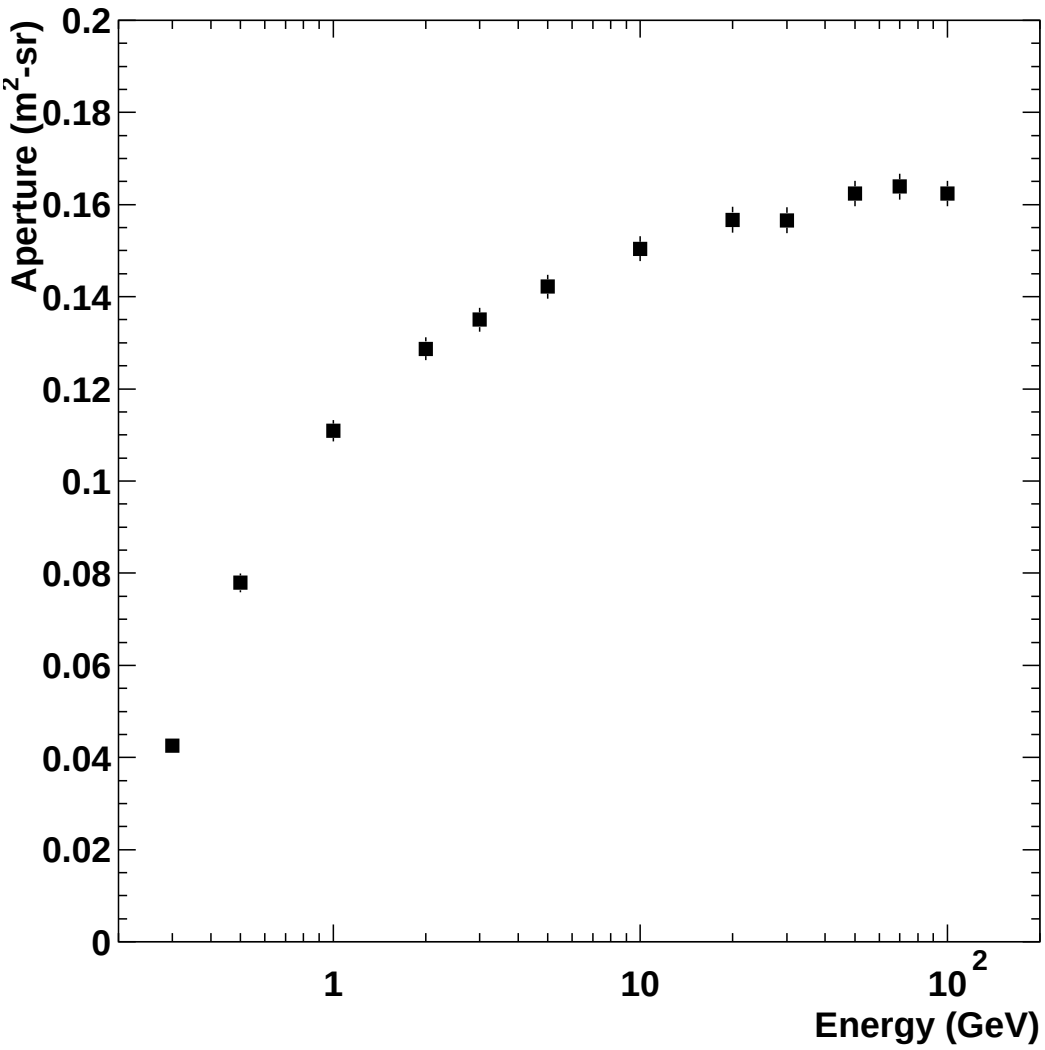

Figure 5: AMS/γ aperture as a function of γ-ray energy. The statistical errors are comparable in size to the circular data points.

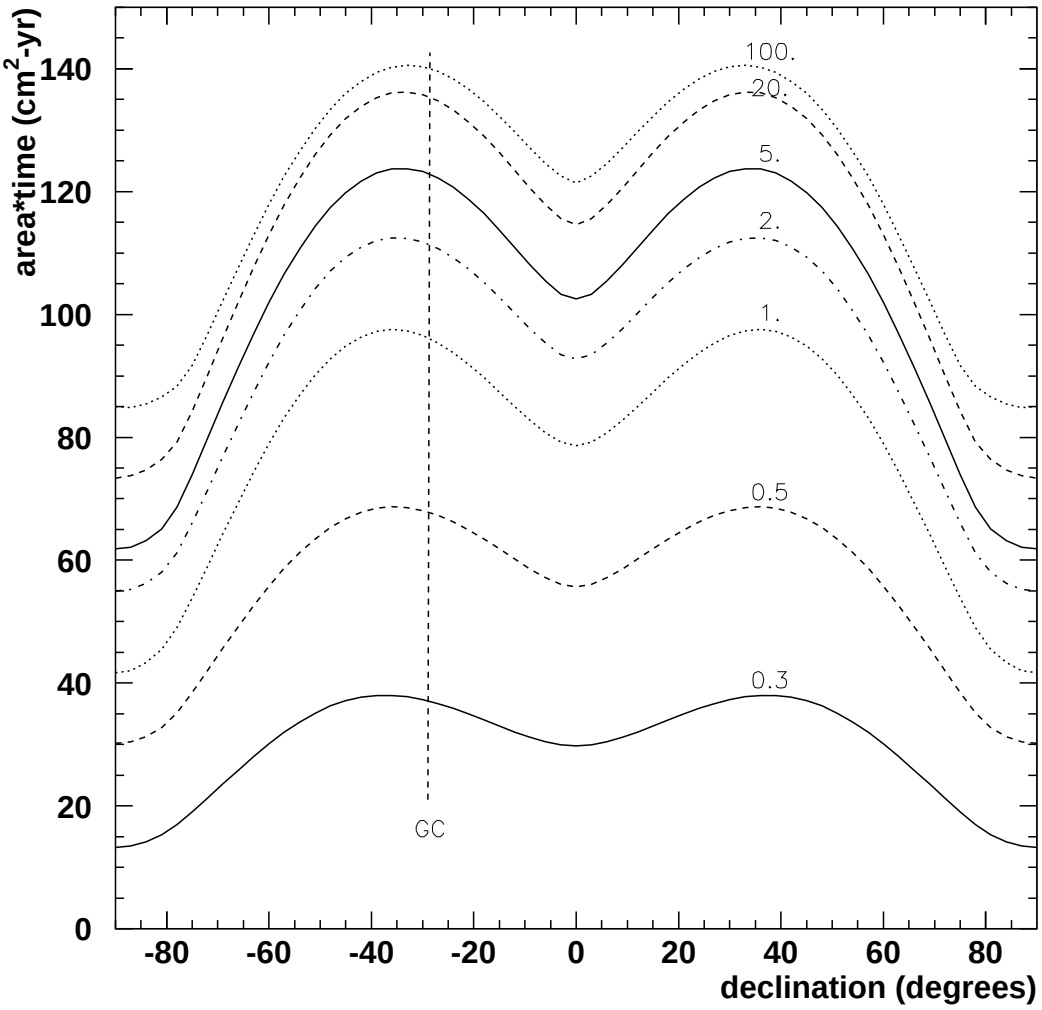

Figure 6: Accumulated area*time product over one year of AMS operation as a function of declination; each curve is marked by the γ-ray energy (in GeV). The declination of the Galactic Center (GC) is also indicated as a dashed vertical line.

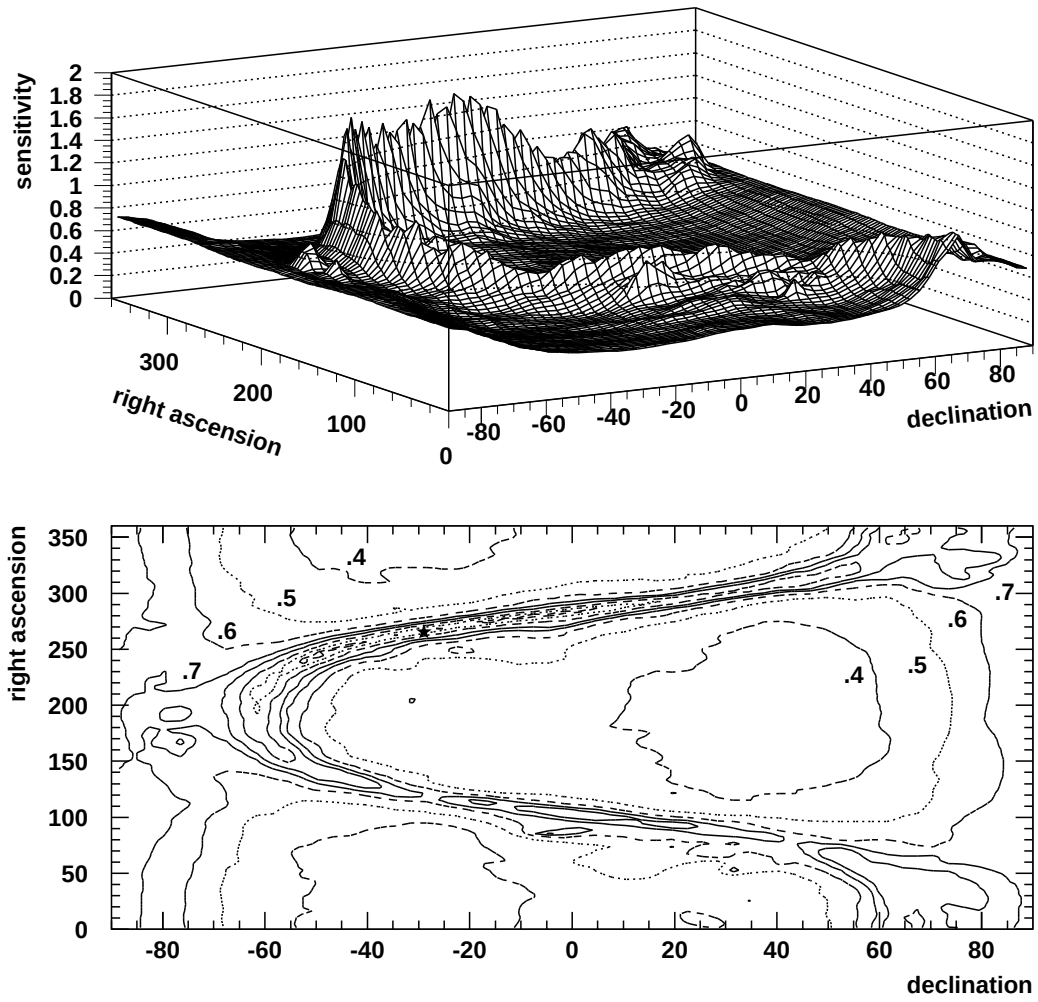

Figure 7: A 3-D plot and 2-D contour plot of AMS/γ's point source sensitivity n_0 versus celestial coordinates. Recall that n_0 is the minimum amplitude of the source's differential flux at 1 GeV required for a 5σ significance detection. The units for n_0 in the 3-D plot are 10^{-8} cm^{-2}·s^{-1}·GeV^{-1}. Large photon fluxes from the diffuse galactic background are responsible for the deterioration of sensitivity near the Galactic plane.

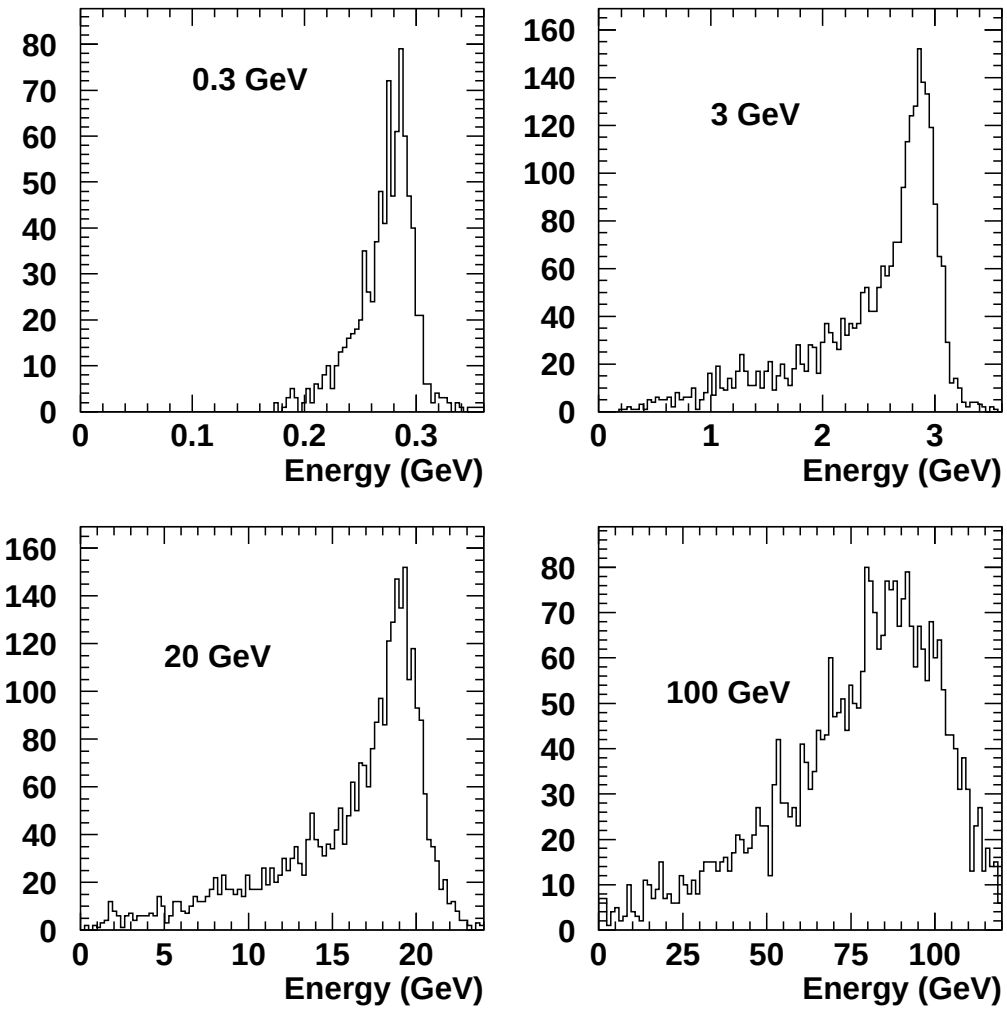

Figure 8: The reconstructed energy distributions for four different primary γ-ray energies, 0.3, 3, 20, and 100 GeV.

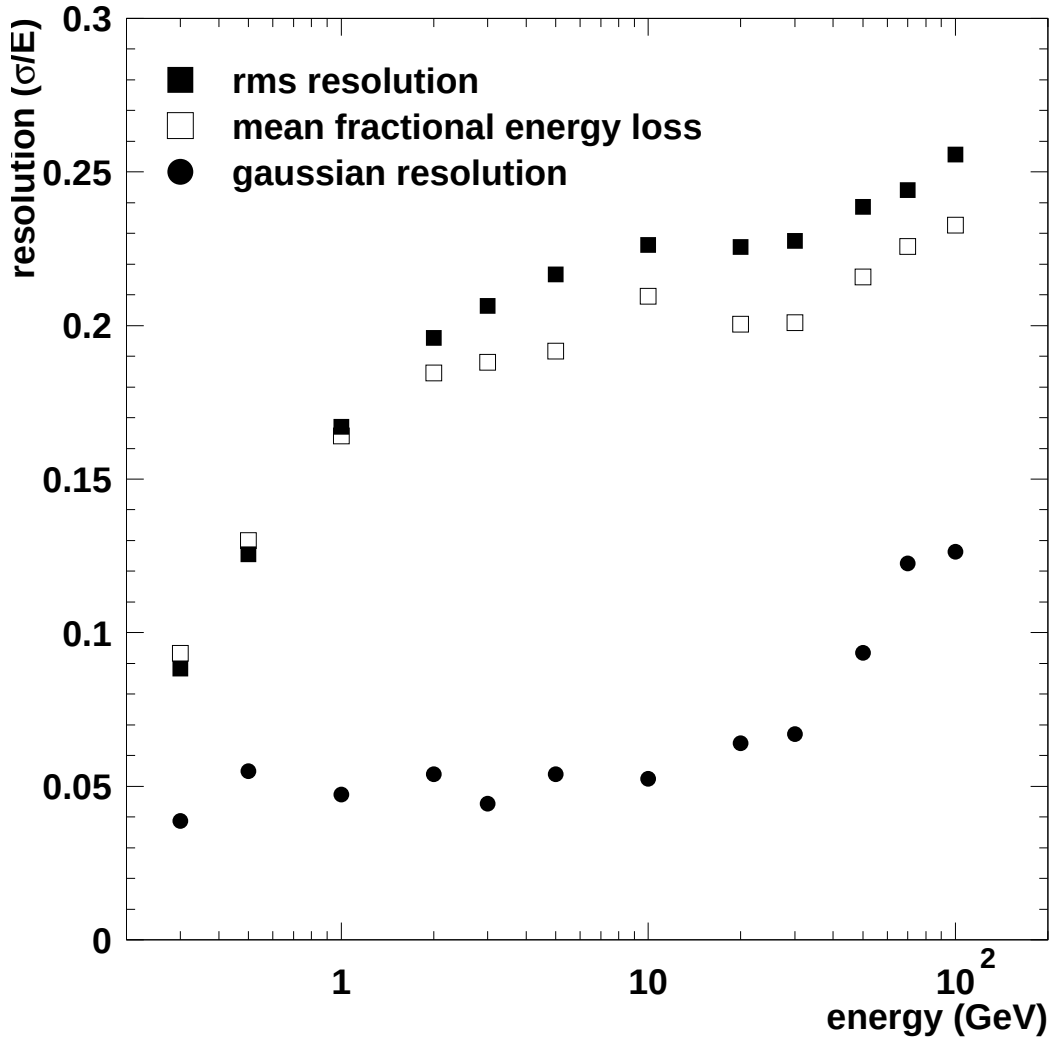

Figure 9: The mean fractional energy loss (open square), rms energy resolution (filled square), and width of the "gaussian" peak of the distribution (filled circle) as a function of primary γ-ray energy.

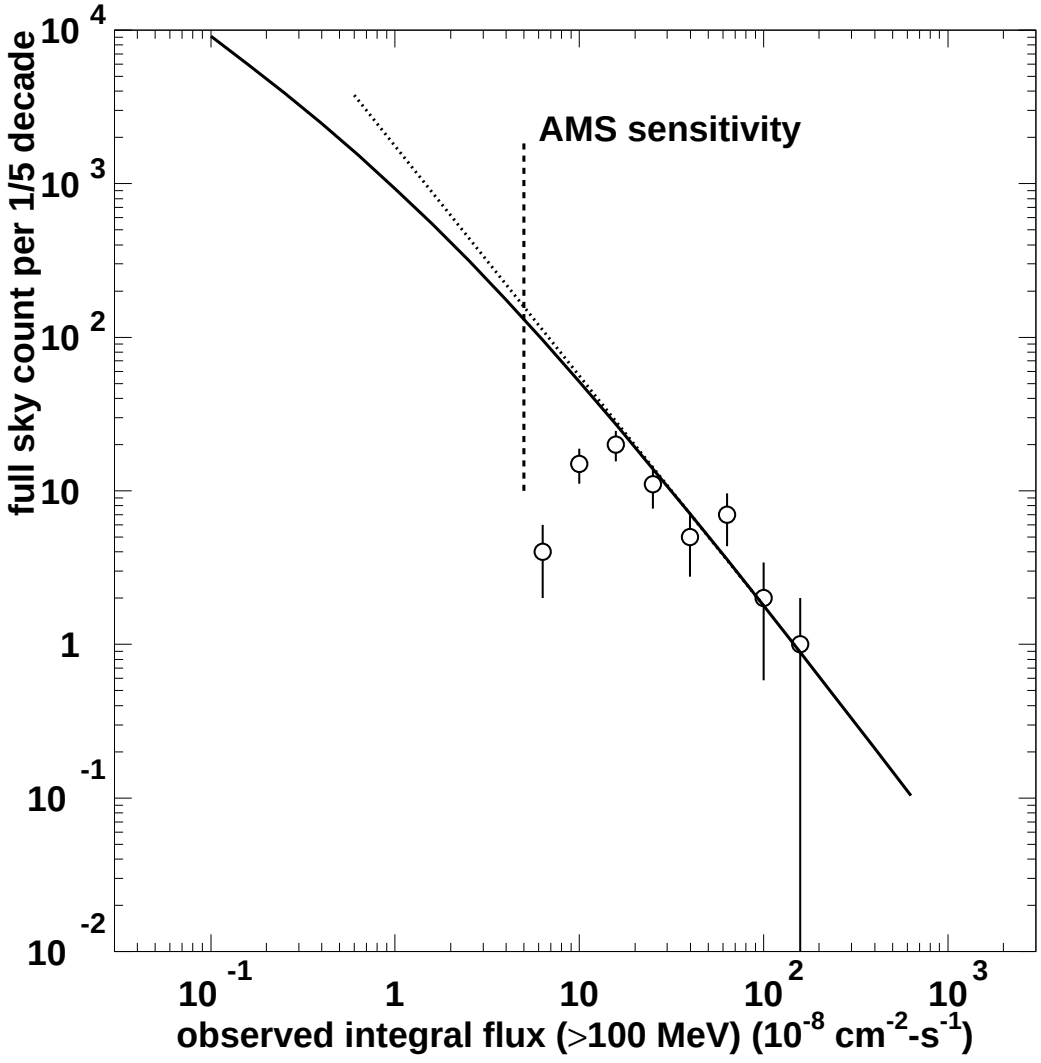

Figure 10: Full sky blazar count as a function of the detected integral γ-ray flux above 0.1 GeV. The ordinate gives the total source counts within *one-fifth*-decade intervals of integral flux. The unfilled circles represent EGRET detections, taken from their Second Catalog [25]; the solid line is the predicted sky count from Stecker and Salamon (1996), and the dotted line is the Euclidean relation, $N(>S) \propto S^{-3/2}$. The dashed line shows the point source integral flux sensitivity of AMS/γ.

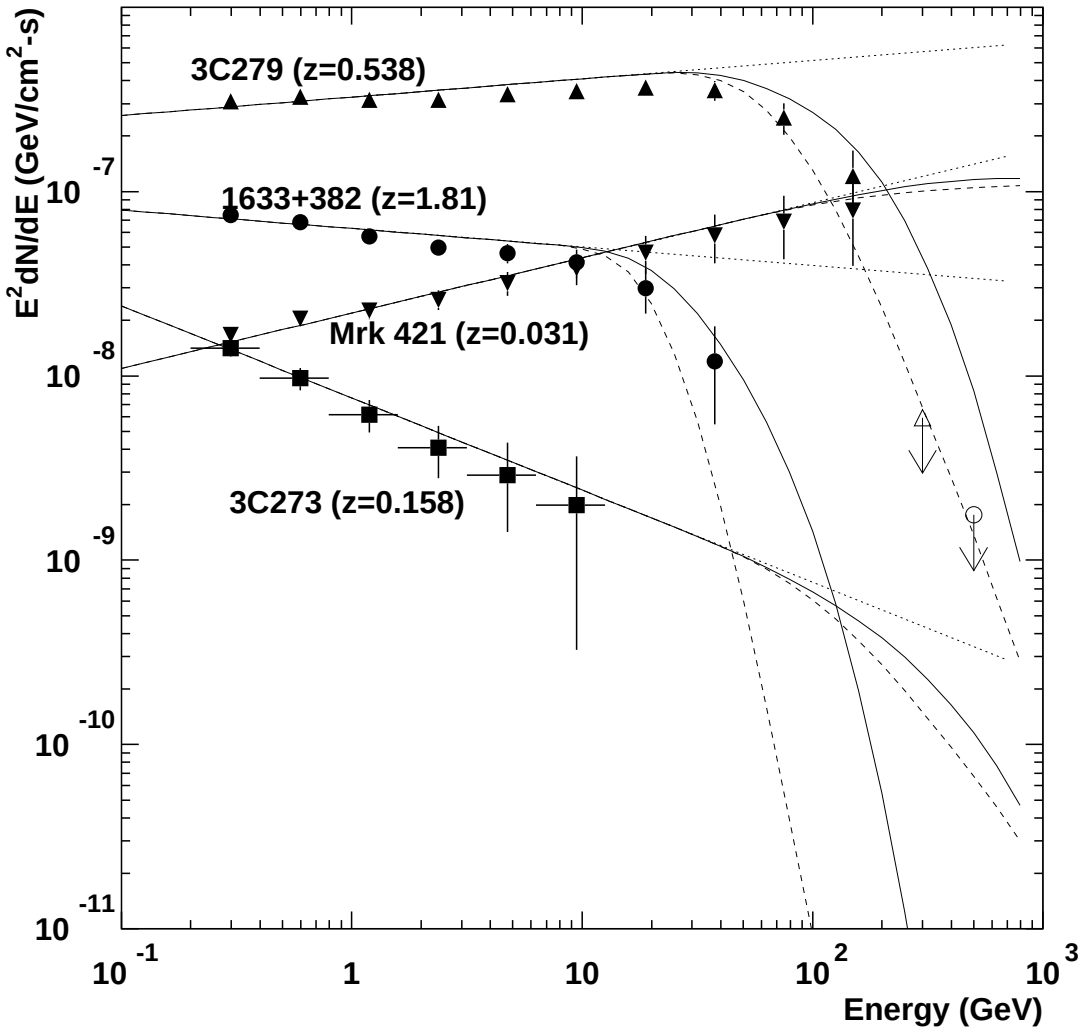

Figure 11: Power law spectra of the blazars 1633+382, 3C273, 3C279, and Mrk 421, extrapolated from the measurements of EGRET. The redshifts z of these sources are indicated in the figure. The dotted lines show the pure power law extrapolation, while the solid and dashed lines show the effect of γ-ray extinction via pair production off the intergalactic soft photon (IR to UV) background according to two different models of the soft photon background [32]. The open triangle and circle represent γ-ray flux upper limits from 3C279 and 1633+382, respectively, as measured by the Whipple Observatory [31]. These are seen to be well below the naive extrapolation of the EGRET power law spectra of these two sources. Note that we show only *one* power-law representation for each source; some sources, such as 3C279, are highly variable, with significant shifts occurring in both the integrated γ-ray flux and spectral index during flare states [9]. Also shown are the expected AMS/γ spectrum measurements corresponding to a two-year integration: 3C279 (filled upper triangles), 1633+382 (filled circles), Mrk 421 (filled lower triangles), and 3C273 (filled squares).

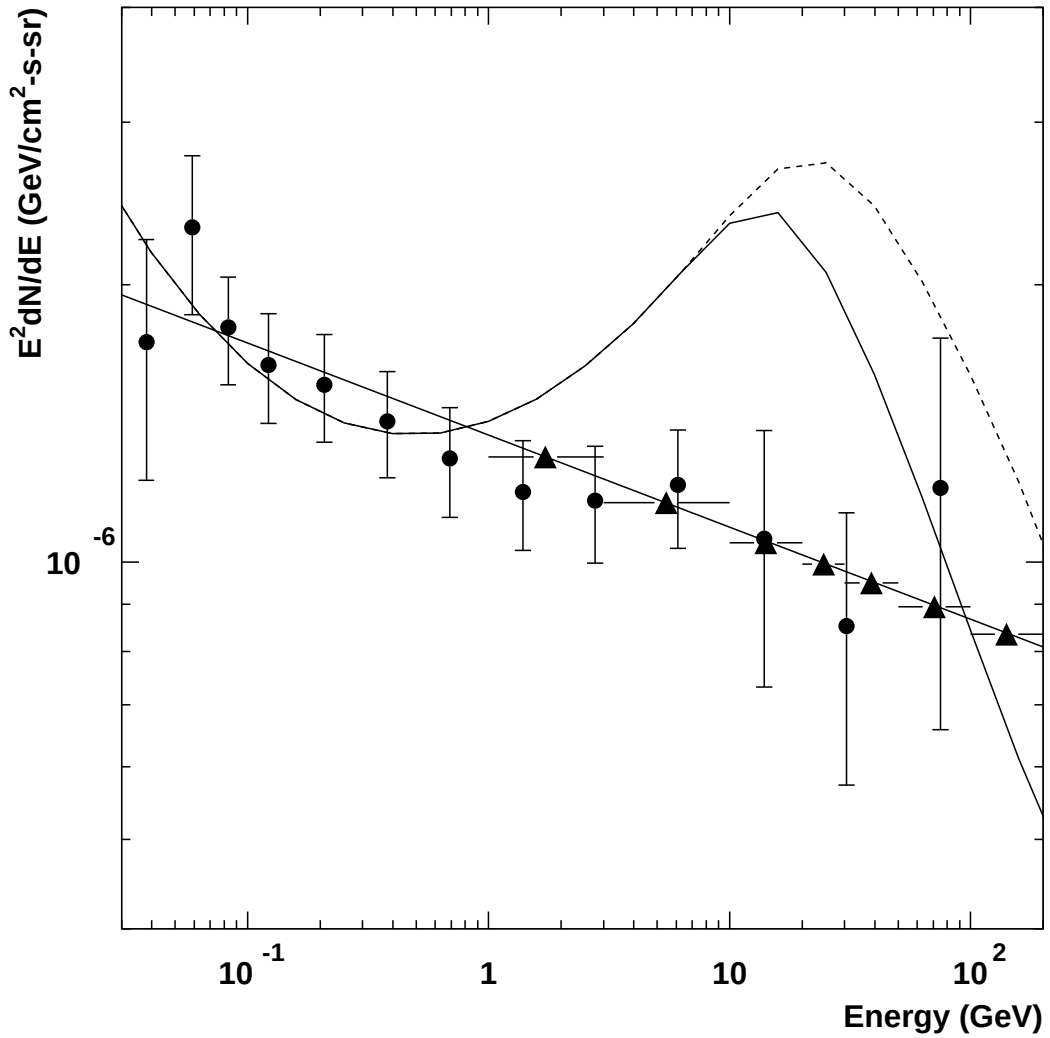

Figure 12: The extragalactic gamma ray background as measured by EGRET (filled circles), along with their fitted (straight solid line) power law spectrum. Also shown are two versions of a theoretical spectrum calculated under the assumption that 100% of the EGRB is due to unresolved blazars [26, 32], which includes the effects of γ-ray attenuation via interactions with the IB optical-to-UV photons. (The solid and dashed line curves differ in assumptions regarding the effects of evolving cosmic metallicity on the optical and UV photon backgrounds.) The peaks in E^2dN/dE at $\sim$ 20 GeV in these theoretical spectra are sensitive to assumptions regarding the spectral index distribution of blazars, which appear to be inconsistent with the EGRET data, but could be readily modified to be more so. The one feature which is *not* malleable is the spectral cutoff at $\sim 20 - 30$ GeV; for an EGRB of blazar-dominated origin a spectral cutoff in the 20-50 GeV region must exist. Should the EGRB spectrum remain a power law out to 100 GeV, the blazar-origin hypothesis would be ruled out. The error bars on the EGRET data (filled circles) are mostly systematic (13% for 0.03 to 10 GeV data; 30% above 10 GeV) [Sreekumar etal 1998], representing over 3 years of EGRET data. AMS *statistical* errors, based on one year of operation, are smaller than the data point symbols (filled triangles). For example, between 50 to 100 GeV, AMS should see 1.3×10^3 EGRB γ-rays in one year, assuming the EGRET EGRB spectrum.

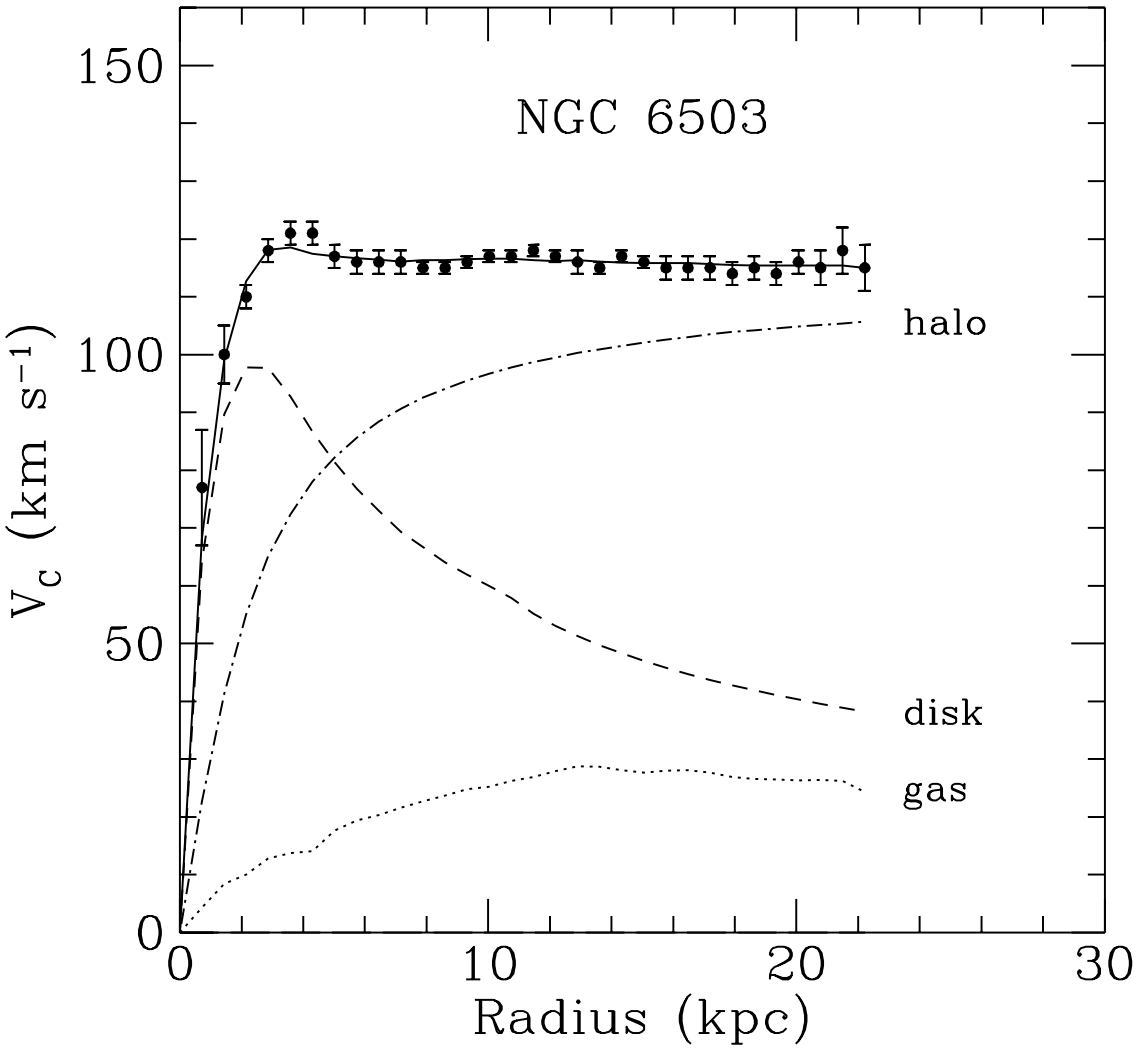

Figure 13: The rotation curve of the galaxy NGC 6503 is shown as a function of radius from the galaxy center, as measured by Doppler shifting of the 21-cm radio line from gaseous HI in the disk. The flatness of the rotation curve at large radii implies an integrated galaxy mass $M(r)$ that falls off roughly as r^{-1}, inconsistent with the observed mass profiles of the visible disk and gas components of the galaxy. The inclusion of a dark matter halo component with density profile $\sim r^{-2}$ provides an excellent fit to the observed rotation curve. This figure is taken from Begeman, Broeils, and Sanders (1991)[80].

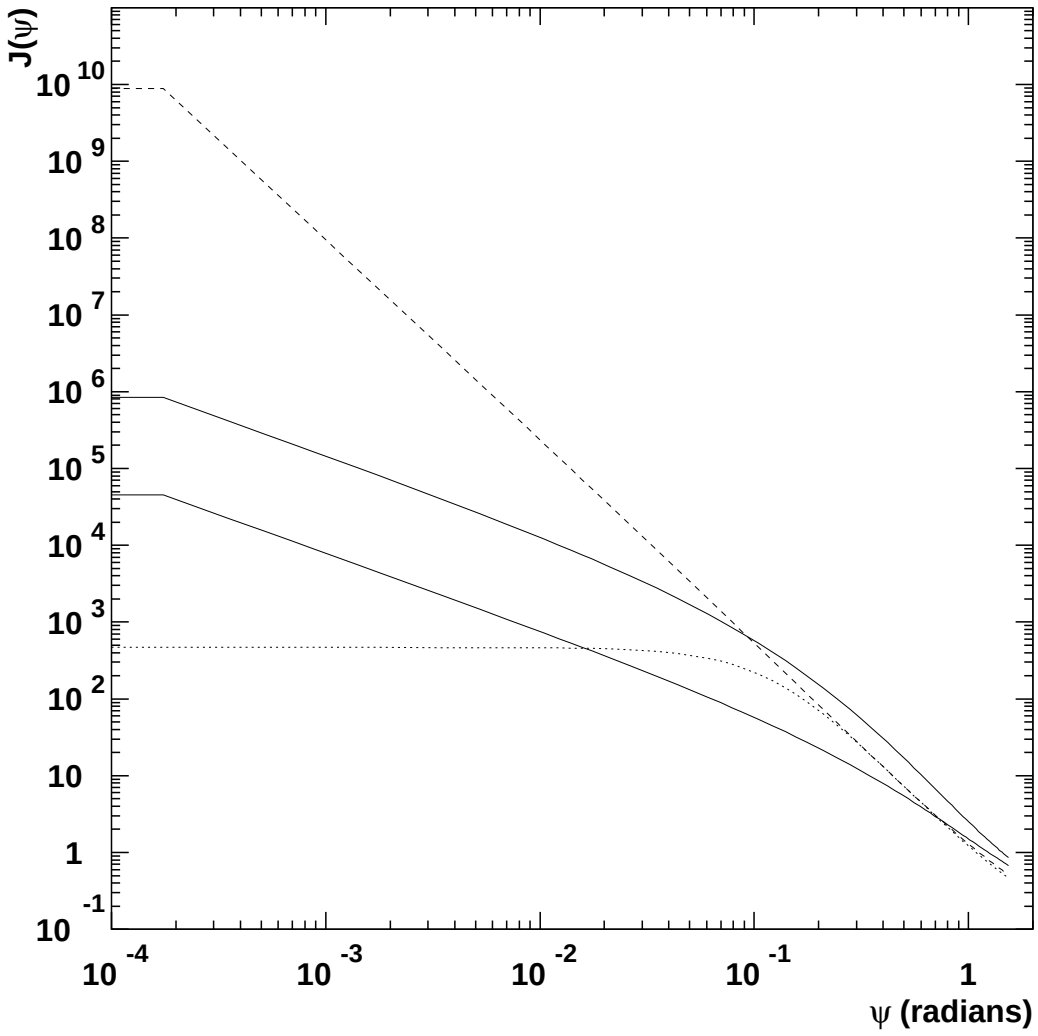

Figure 14: The integrated γ-ray flux $J(\psi)$ versus the angle ψ from the Galactic center for the tabulated halo dark matter density profiles, where $J(\psi)$ is defined in Eq. 12. The dashed, upper and lower solid, and dotted lines correspond respectively to D&B models 2f, 4d, 2d, and the quasi-isothermal halo profile. The most optimistic profile is model 2f, which is very close to that of Berezinsky et al (1992). Models 4d and 2d are both NFW halo profiles.

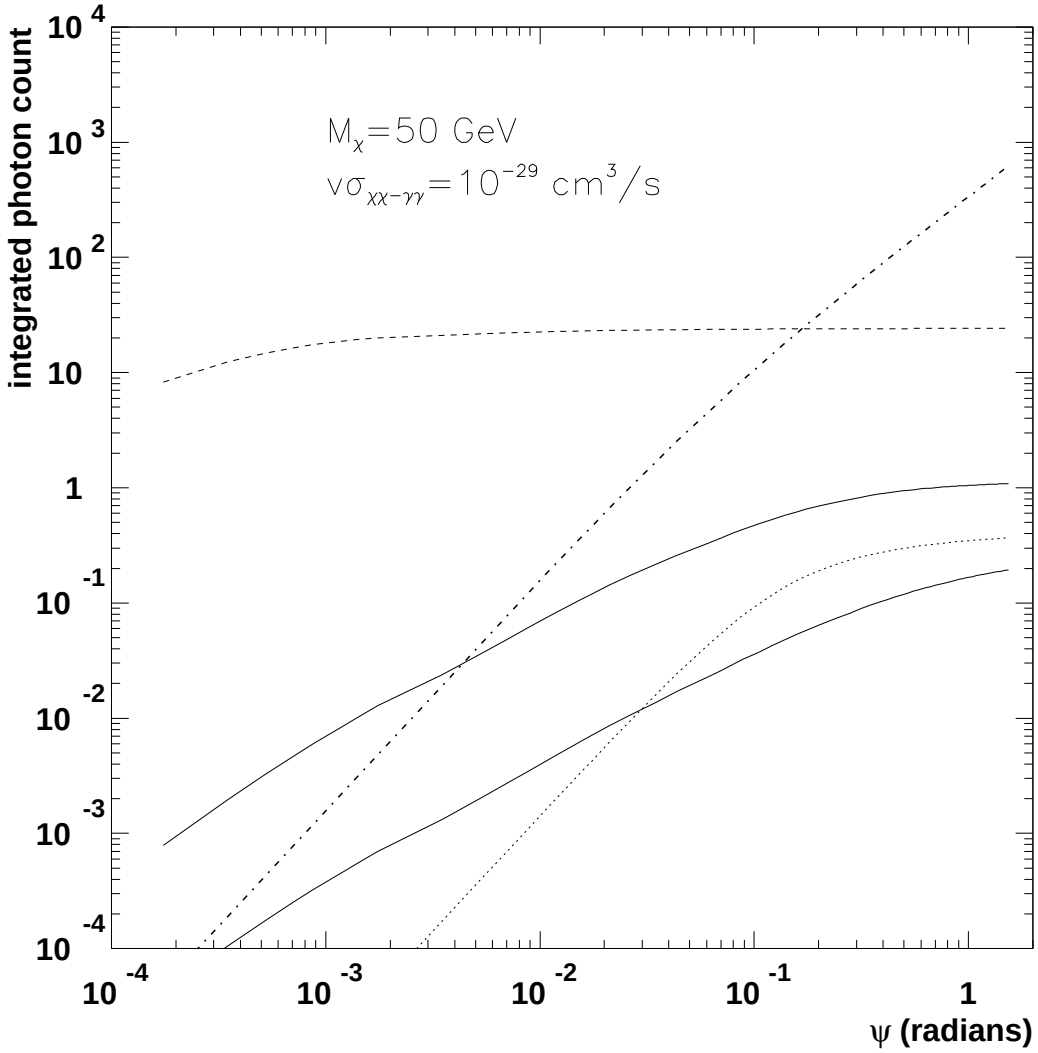

Figure 15: Integrated γ-ray counts $N(<\psi)$ as a function of angle ψ (in radians) from the galactic center, assuming $M_\chi = 50$ GeV, producing a narrow line at $E_\gamma = 50$ GeV. See discussion in text.

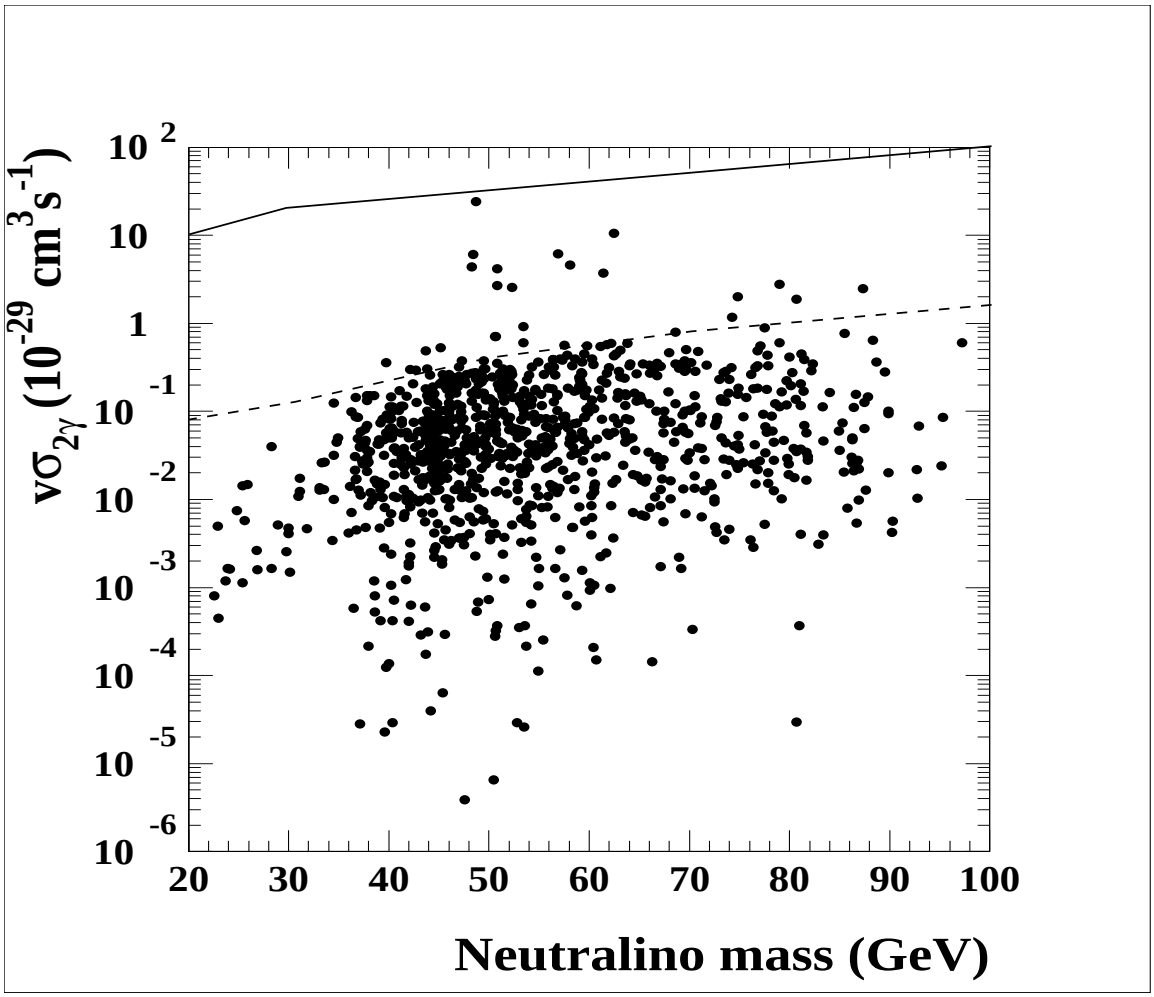

Figure 16: The velocity-cross section product required for AMS detection of a neutralino induced γ-ray line as a function of neutralino mass and halo profile model. The dashed line corresponds to D&B model 2f, which is the "Berezinsky-like" model; the solid line corresponds to D&B model 4d, the more productive of the two "NFW-like" halo profiles. These curves are superimposed on Fig. 3a of Bergström and Ullio (1997), which gives their calculated cross sections based on a scan of SUSY parameter space.

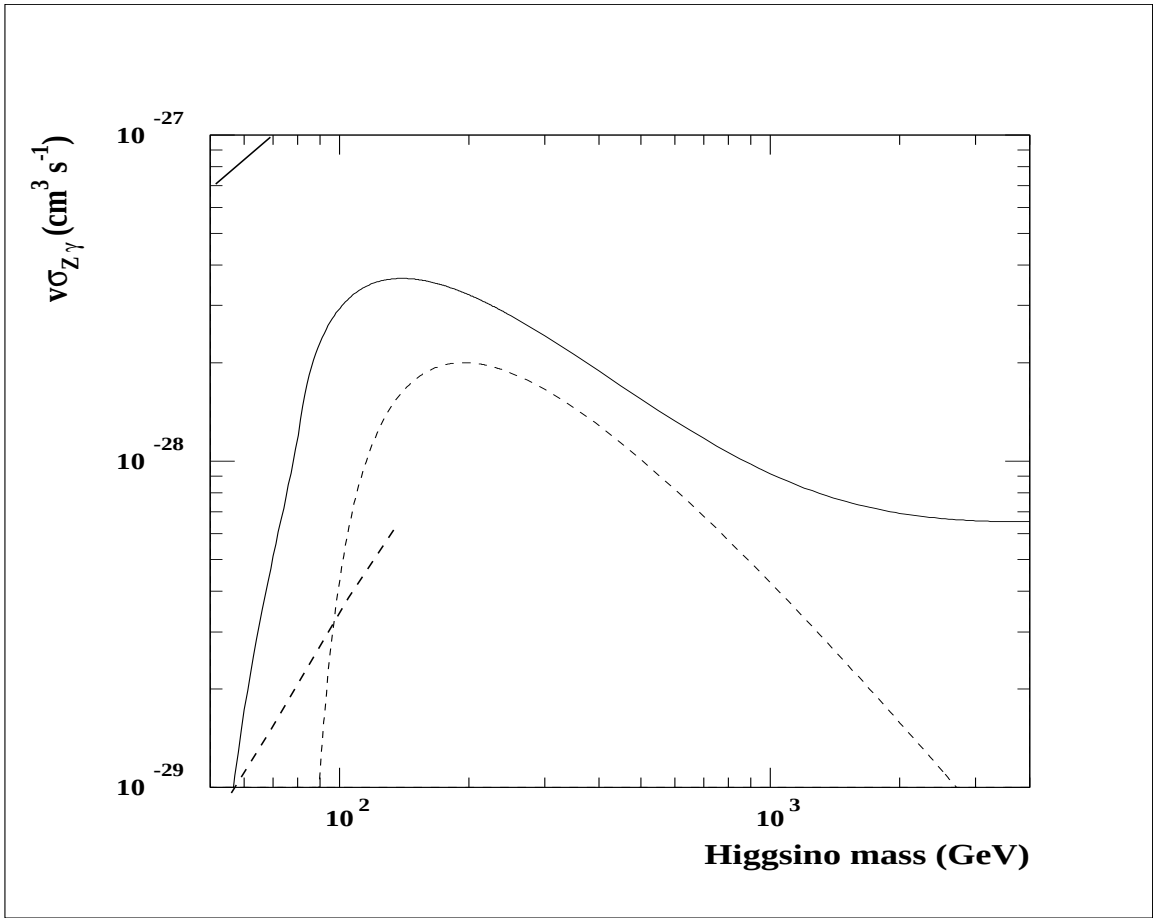

Figure 17: The velocity-cross section product required for AMS detection as a function of neutralino mass and halo profile model. These curves are from Fig. 6 of Ullio and Bergström (1997), which gives their calculated cross section for the single-photon production channel $\chi\chi \to \gamma Z$ or a pure higgsino state. The dashed-line line segment corresponds to D&B model 2f, which is the "Berezinsky-like" model. The other halo profiles do not intersect the Ullio and Bergström curves. (The solid line segment in the upper-left corner corresponds to D&B model 4d.)

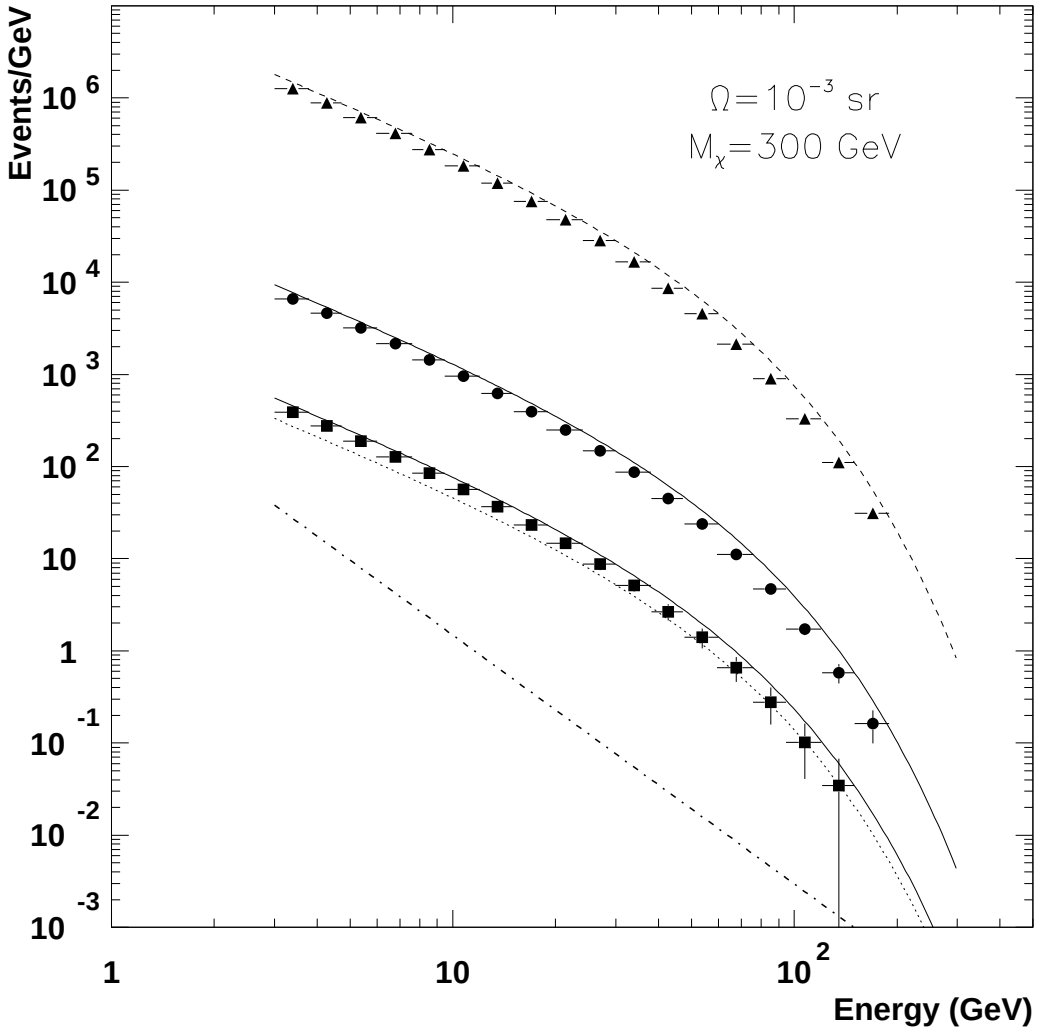

Figure 18: The differential continuum γ-ray event count from neutralino (higgsino) annihilation in the Galactic halo detected by AMS over a 2-year time period, within a solid angle of 10^{-3} sr about the Galactic center, based on the cross sections for $\chi\chi \to WW, ZZ$ of Bergström, Ullio, and Buckley [74]. The dashed, upper and lower solid, and dotted lines correspond to the various halo models: Models 2f, 4d, 2d, and quasi-isothermal, respectively. The dot-dashed line shows the sum of the integrated diffuse galactic and extragalactic γ-ray background γ-rays detected by within the same solid angle. The faux-data points show the energy bin counts obtained by AMS after convolution with the energy resolution function of the detector. (Faux data points are not shown for the quasi-isothermal halo model.)

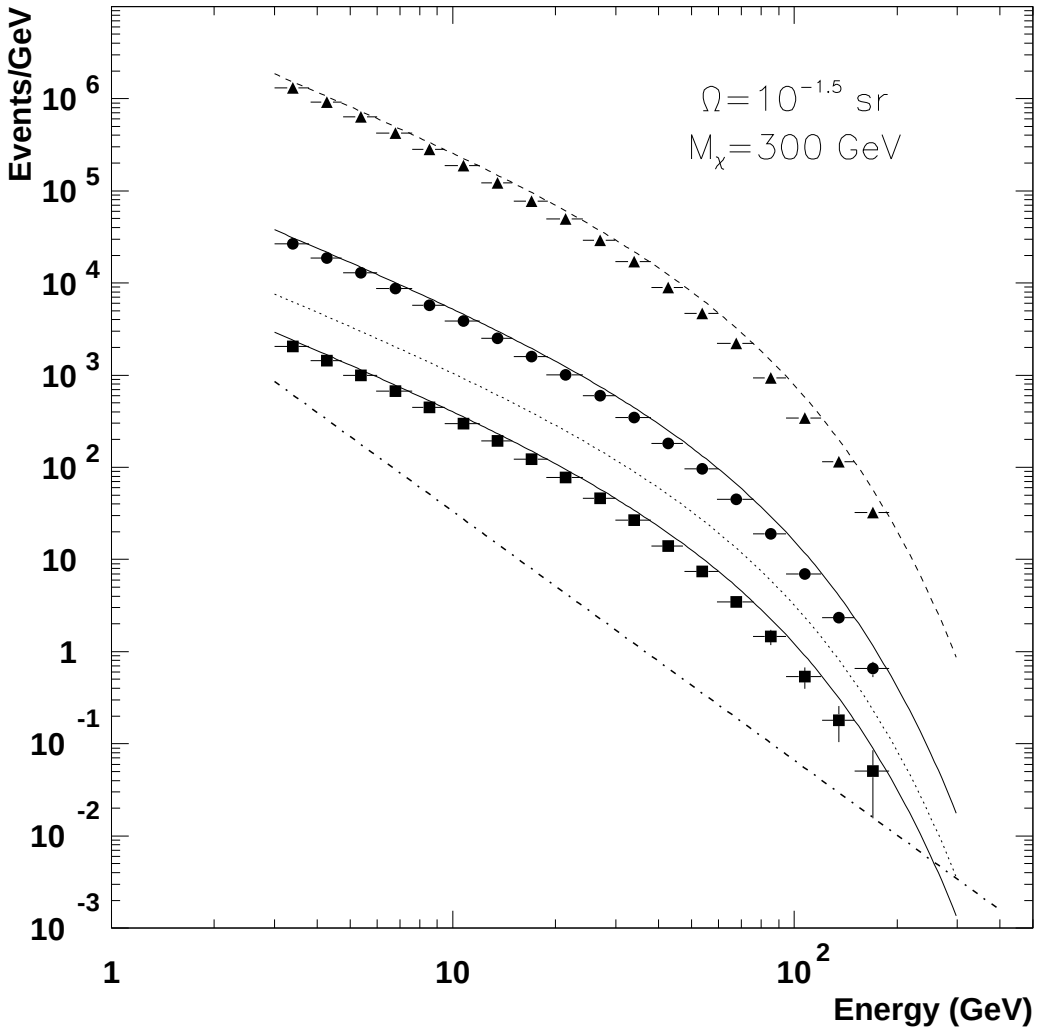

Figure 19: The same as Figure 18, except the fluxes are those that arrive within a solid angle of 0.03 sr about the Galatic center.

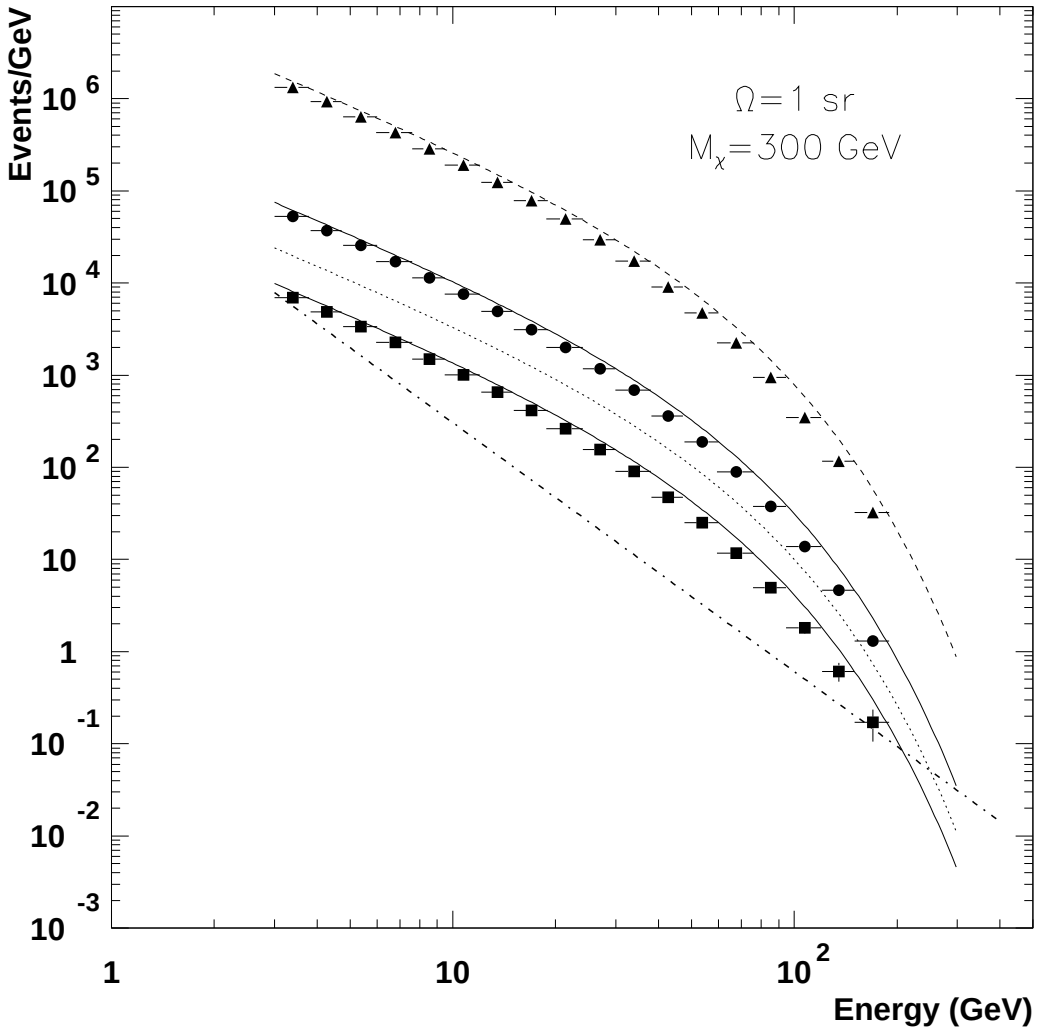

Figure 20: The same as Figure 18, except the fluxes are those that arrive within a solid angle of 1 sr about the Galatic center.